Diffusion as the main process for mass transport in very low water content argillites: 1. Chloride as a natural tracer for mass transport—Diffusion coefficient and concentration measurements in interstitial water

Delphine Patriarche,[1,2] Jean-Luc Michelot,[3] Emmanuel Ledoux,[1] and Sébastien Savoye[4]

Received 16 August 2003; revised 4 November 2003; accepted 13 November 2003; published 21 January 2004.

[1] Argillites are one of the rock types studied by French authorities for their confining properties for the isolation of radioactive wastes. One of the main objectives of such study is the better understanding of water transport through rocks with very low water content and hydraulic conductivity, using modeling of tracer profiles. This article presents the protocol developed and applied for acquiring data on chloride in interstitial water of the Toarcian argillites in Tournemire (southern France). This protocol is based on laboratory experiments involving diffusion process and on modeling. Experimental data obtained during transient and steady parts of diffusion allow for the assessment of the diffusion coefficient and initial concentration in pore water, respectively. Profiles for both have been acquired along the geological sequence; they are used in part 2 of this article for proposing a hydrogeological model where diffusion appears to be the main process for mass transport through the argillites and for comparing deuterium and chloride transport. *INDEX TERMS:* 1094 Geochemistry: Instruments and techniques; 1040 Geochemistry: Isotopic composition/chemistry; 1832 Hydrology: Groundwater transport; 5114 Physical Properties of Rocks: Permeability and porosity; 5139 Physical Properties of Rocks: Transport properties; *KEYWORDS:* interstitial water, porosity, chloride, data acquisition, diffusion coefficients, transport

Citation: Patriarche, D., J.-L. Michelot, E. Ledoux, and S. Savoye (2004), Diffusion as the main process for mass transport in very low water content argillites: 1. Chloride as a natural tracer for mass transport—Diffusion coefficient and concentration measurements in interstitial water, *Water Resour. Res.*, *40*, W01516, doi:10.1029/2003WR002600.

1. Introduction

[2] In the last two decades, sitings of possible nuclear waste repositories have been the object of intense debates within the biggest producing countries of nuclear energy such as the United States, Japan, United Kingdom, and France. While most experts agree that such repositories should be placed in deep geological locations, opinions differ concerning the optimal geological setting [*Brookins*, 1984]. One major issue with the conceptualization of nuclear waste repositories is that all safety scenarios must be considered over very long periods of time (thousands to millions years) due to the extreme long half-life of transuranians and fission products. Obviously, one of the major points related to such storage has to do with the water flow regime in the area of the repository and with how this flow regime would affect or enhance the transport of radioelements in case of an eventual leak from the repository occurs.

[3] While the United States is considering storage of nuclear wastes in volcanic sequences, in a fractured media at a level above the water table, at the Yucca Mountain site [*Sonnenthal and Bodvarsson*, 1999; *Stuckless and Dudley*, 2002], France is considering placing its major nuclear waste repository at depth in saturated media well below the water table [*Lebon and Mouroux*, 1999]. French authorities consider argillite formations as the possible safest choice for such repository because they have extremely low vertical and horizontal hydraulic conductivities; consequently, the horizontal and vertical water movement able to transport radionuclides to other locations [*Hoteit et al.*, 2000], would be extremely slow. Thus ANDRA (French agency in charge of radioactive waste management) recently decided to build an underground research facility at Bure (east of the Parisian Basin), in Callovo-Oxfordian units, in order to evaluate the safety for these repositories.

[4] The IRSN (French Institution for Radioprotection and Nuclear Safety, formerly IPSN) is in charge of an independent expertise for industrial (ANDRA's) projects. In order to conduct methodological research on the feasibility of storing radioactive wastes in deep clayey massifs, the IPSN selected in 1988 the argillaceous units (Upper Lias) of the Tournemire massif (Aveyron, southern France) for installing an underground experimental facility.

[5] Obtaining accurate information on the water flow in porous media with very low hydraulic conductivities and water content using only traditional hydrogeological methods is extremely difficult. This usually leads to com-

[1]Ecole Nationale Supérieure des Mines de Paris, UMR 7619, Fontainebleau, France.
[2]Now at Department of Geological Sciences, University of Michigan, Ann Arbor, Michigan, USA.
[3]OrsayTerre, FRE 2566 CNRS, Faculté des Sciences, Université de Paris-Sud, Orsay, France.
[4]Institut de Radioprotection et de Sûreté Nucléaire, Fontenay-aux-Roses, France.

0043-1397/04/2003WR002600

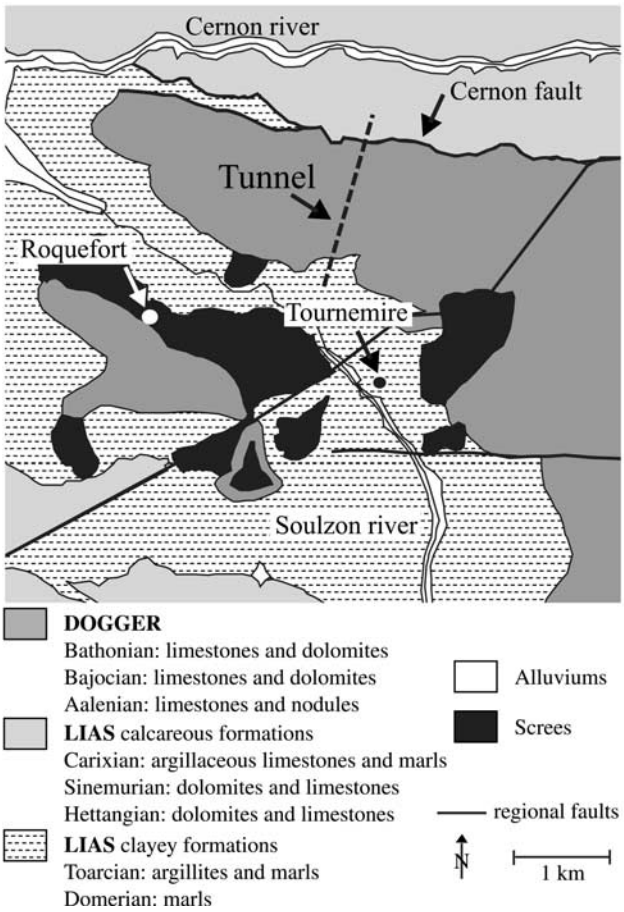

Figure 1. Location of the Tournemire site: simplified geological map after *Mennessier and Collomb* [1983].

bine geochemical information with hydrogeological methods. However, transfer time of artificial tracers are too long in such media and obtaining information therefore requires data on natural tracers, which may record media history over long periods of time [*Desaulniers et al.*, 1981; *Falck et al.*, 1990; *Harrington et al.*, 2001; *Stone*, 1992; *Toulhoat et al.*, 1996; *Tyler et al.*, 1996]. The distribution of natural tracers in interstitial water of formations may help to characterize water flow and solute transport through the media.

[6] Because of its conservative behavior [*Michard*, 1982], chloride is one of the most common chemical tracers [*Eggenkamp*, 1998], and was therefore chosen for investigating mass transport in the hydrogeological system of the Tournemire massif. In order to obtain high-quality measurements of chloride (or any other tracer) in pore water of argillaceous rocks, many scientists have developed and improved various techniques [*Sacchi et al.*, 2000, 2001]. One of the most recent is that developed by *van der Kamp et al.* [1996] using direct chemical equilibration of the interstitial water through a liquid phase; this method was validated by comparing interstitial water concentrations calculated after equilibration with concentrations measured in ''free'' water collected by piezometers in the same formation. Good agreements were obtained for deuterium and sulfate, but the method was not able to give consistent results for chloride [*van der Kamp et al.*, 1996]. For this reason, and because in the Tournemire case comparison with chloride concentration of free water was not possible (except locally, where water comes from faults, which may not be representative of interstitial water), others methods were tested. For instance, water extraction by applying a very high stress on the rock sample [*Reeder et al.*, 1998], was tested on Tournemire argillites by the British Geological Survey. This technique was not reliable because addition of water to the rock sample was necessary, and this created several nonnegligible artifacts, such as dissolution of carbonates, ionic fractionation and modification for exchangeable bases [*Cave et al.*, 1997; *De Windt et al.*, 1999]. A leaching technique was also tested; results show that chloride extracted by this technique is fifteenfold less than total chloride content of the rock [*Moreau-Le Golvan*, 1997; *Moreau-Le Golvan et al.*, 1997]. In order to obtain good measurements of chloride concentrations in interstitial water of Tournemire argillites, the development of a new protocol appeared indispensable.

[7] Here we present a combination of experiments and analyses for evaluating the various reservoirs of chloride in the rock (including interstitial water); the protocol allows for the determination of both chloride pore water concentration and diffusion coefficients. Assessment of chloride diffusion coefficients through the rock is essential because we expect diffusion to be a major phenomenon in mass transport, considering the very low hydraulic conductivity values of the media.

[8] After describing the geological setting of the Tournemire site, we present laboratory results and modeling of diffusion experiments used in establishing the protocol. We then present data acquired using the protocol and discuss their relevance to mass transport through the Tournemire argillites.

2. Geological Settings and Implications for Hydrogeology

[9] The Tournemire site is located in southern France (about 120 km north of Montpellier), on the western border of the Causses Basin (Figure 1), a Mesozoic sedimentary (marine) basin that constitutes the southern border of the French Massif Central.

[10] Sedimentary units of the Tournemire massif are subhorizontal (Figure 2). In the area of interest, three Lower to Middle Jurassic units are distinguished. The lower (Hettangian, Sinemurian, and Carixian in the Lias) and the upper units (Upper Aalenian, Bajocian, and Bathonian in the Dogger) consist of karstic limestones and dolomites. The intermediate unit (Domerian and Toarcian in the Upper Lias) is marl and shale. The Lower, Middle, and Upper Toarcian consist of 25 m of very indurated shale, 20 m of marl, and 160 m of argillites, respectively. To the north, the Cernon fault interrupts the geological sequence and sets Toarcian argillites on contact with Trias layers; this fault, which shows a regional extension, constitutes a flow path for karstic water between the calcareous units of the massif.

[11] Upper Toarcian units are crossed by an old railway tunnel, drilled more than one hundred years ago, from which several series of boreholes (mostly vertical such as DC, CA, TN1, TN3...) have been drilled; eight radial boreholes (ID) (see vertical boreholes in Figure 3a) and two horizontal galleries were also drilled. These show the

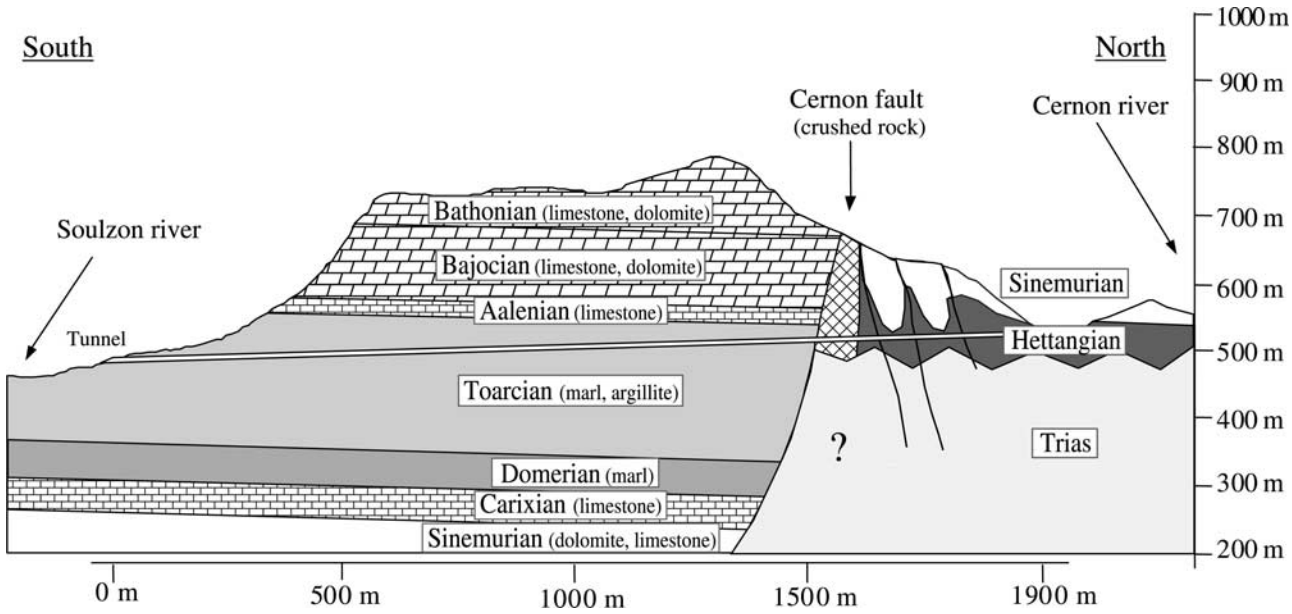

Figure 2. Vertical cross section of the Tournemire massif showing the Trias and Jurassic successions interrupted by the Cernon fault; investigation of the Tournemire massif was performed by drilling boreholes upward and downward from the tunnel crossing the Upper Toarcian, after *Boisson et al.* [1998b].

western part of the massif to be well fractured and the eastern part to be poorly fractured (Figure 3b). Three other descending boreholes (VF2, VF3 and VF4) were drilled along the eastern gallery.

[12] In order to compare data from various boreholes, and to place each sample to its lithostratigraphic unit, slopes of the tunnel and the geological layers were taken into account; knowing elevations of drilling heads, and elevations of stratigraphic transitions, a corrected elevation was calculated for each sample. Later, we present chloride concentration profiles along corrected elevations where the TN1 and TN3 boreholes are taken as reference.

[13] Several fault types, linked to various tectonic events [*Boisson et al.*, 1998b; *Cabrera*, 1992], affect the massif. Major deformations occurred during the N/S Pyrenean compression between 53 and 33 million years ago (paroxysm about 42 million years ago). This compression created most of the fractures (NNW-SSE) with strong slopes such as

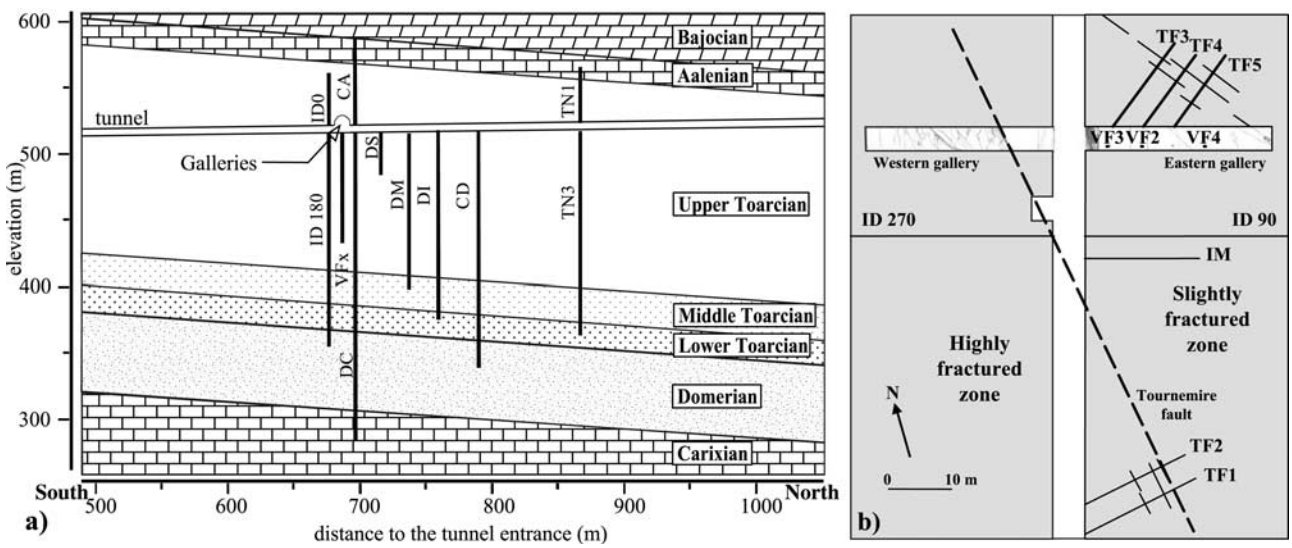

Figure 3. (a) Vertical cross section of the Tournemire massif, showing the locations of vertical boreholes and galleries in the tunnel, and (b) horizontal cross section indicating the location of the descending boreholes drilled in the eastern gallery and the vertical main fault of the Tournemire massif separating the massif into the highly fracture area on the western part and slightly fractured area on the eastern part, after *Boisson et al.* [1998b].

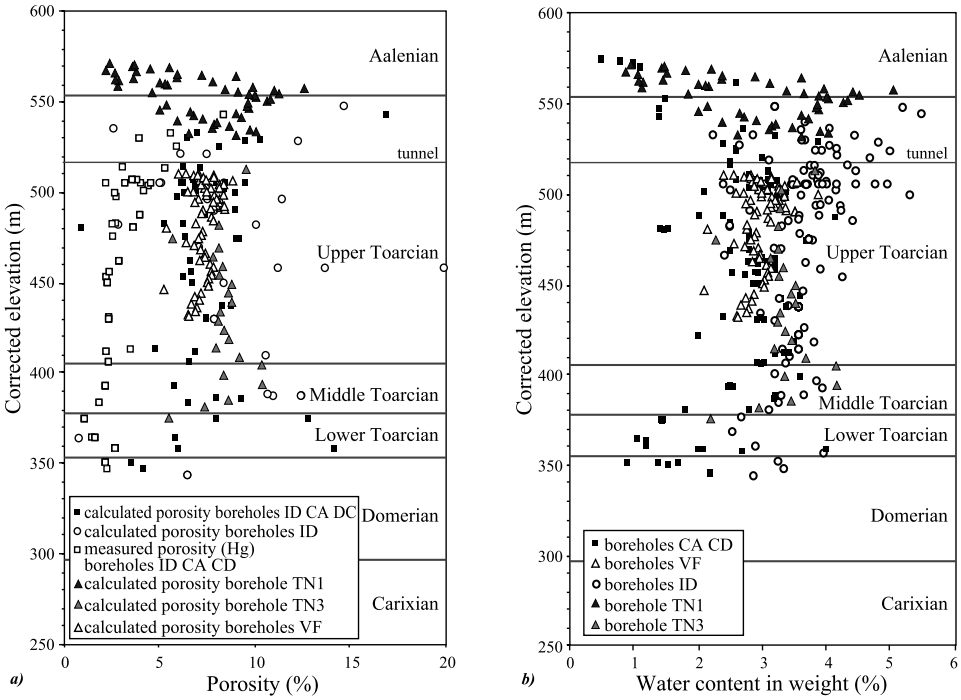

Figure 4. Vertical profiles of the measured and calculated (a) porosity and (b) water content in weight at the Tournemire site (data from *Boisson et al.* [1998b] and this study).

the Tournemire fault (Figure 3b), and it also reactivated the main regional faults (mainly E/W) including the Cernon fault.

[14] Because most faults date from the Pyrenean compression, and because the Cernon fault preceded them, argillites probably acquired their rigidity and subsequent susceptibility to fracturing under mechanical stress quite early in the massif history. This was probably due to a major loss of water from these argillites during sedimentation and burial. However, despite the fact that argillites are water saturated [*Barbreau and Boisson*, 1994], they have a very low porosity (7% in average) and a very low water content (about 3–5% in weight). The water content θ was calculated as $\theta = \frac{\text{wet mass} - \text{dry mass}}{\text{wet mass}}$ (after drying at 105°C, during 24 hours) and the porosity ω_θ was calculated with $\omega_\theta = \theta \times \frac{\text{wet rock density}}{\text{water density}}$ (Figure 4), with a wet rock density value of 2500 kg m^{-3} [*Boisson et al.*, 1998c].

[15] Hydrogeology of the Tournemire site is mainly controlled by permeability contrasts between karstic aquifers and Toarcian and Domerian (argillite/marl) layers. The upper karstic aquifer is located in Middle Jurassic layers (often just Aalenian); it is recharged by local precipitation on the plateau that seep into Bathonian and Bajocian layers, via pathways created by the dissolution of carbonates along faults. Porosities of these calcareous layers, and their water contents are very variable. The deeper karstic aquifer is in the Hettangian, Sinemurian and Carixian series, extending down to Trias layers, which relatively constitutes an impermeable substratum. This aquifer has a regional extension and crops out south of the study area.

[16] The hydraulic head h of the Aalenian aquifer (602 m at the elevation z 588 m, corrected elevation z_c 574 m) is higher than that of the Carixian aquifer (463 m at z 296 m, z_c 283 m), suggesting a potential downward leakage toward this aquifer [*Boisson et al.*, 1998a; *Cabrera et al.*, 2001; *Patriarche*, 2001]. The vertical hydraulic gradient $\frac{\Delta h}{\Delta z}$ between the top and the bottom of the argillites is 0.48 m m^{-1}; this high value is a consequence of the low hydraulic conductivities of this material.

[17] In Toarcian/Domerian rocks, in situ pulse tests and laboratory measurements provided hydraulic conductivities ranging between 10^{-11} and 10^{-13} m s^{-1} for the fractured areas and between 10^{-14} and 10^{-15} m s^{-1} for nonfractured argillite [*Boisson et al.*, 2001]. In fractured areas, in situ tests have been performed at various scales. A test using the method of *Bredehoeft and Papadopulos* [1980] between 57.0 and 160.15 m below the tunnel (including fractured and nonfractured levels) showed a hydraulic conductivity K value of 1.4×10^{-14} m s^{-1}. Several other tests using the method of *Wang et al.* [1977] performed along specific fractured areas (with a 1.5 m thickness) showed transmissivities ranging between 10^{-13} and 2×10^{-12} m^2 s^{-1} with fracture apertures of 0.17 and 0.1 mm and hydraulic conductivities of 5.88×10^{-13} and 10^{-13} m s^{-1}, respectively. Measurement between 41.5 and 43.0 m below the tunnel yielded $K = 2.3 \times 10^{-11}$ m^2 s^{-1} using the method of *Bredehoeft and Papadopulos* [1980]. These hydraulic conductivities are in agreement with the orders of magnitude given by *Neuzil* [1994] for the Pierre Shale in South Dakota (clay stone), Lower Cretaceous in Western Canada (clayey siltstone), and Eleana Formation in Nevada (argillites). The Peclet number P_e given by

$$P_e = \frac{U\sqrt{k}}{\omega_\theta D_0} = \frac{K\frac{\Delta h}{\Delta z}\sqrt{\frac{\mu K}{\rho g}}}{\omega_\theta D_0}$$

Table 1. VF4 Borehole Samples Used for PECH Elaboration: Label, Vertical Distance From the Tunnel, and Elevation of the Samples and, for Each Sample, Water Content in Weight, Water Content Porosity, Geochemical Porosity for Chloride, Rock/Water Ratio for the Associated Diffusion Experiment

Sample	Vertical Distance From the Tunnel, m	Elevation, m	θ, %	ω_0, %	ω_{geoch}, %	R/W, g L^{-1}
VF4 06070	60.70	457	3.13	7.8	2.33	2272
VF4 06465	64.65	453	3.15	7.9	2.33	2266
VF4 06875	68.75	449	3.11	7.8	2.33	2267
VF4 07260	72.60	445	3.11	7.8	2.33	2265
VF4 07670	76.70	441	2.50	6.3	1.88	2270

[see, e.g., *de Marsily*, 1986] indicates the nature of the fluid flow (and its relative importance to diffusion), which depends on Darcy velocity U (m s^{-1}), permeability k (m^2) or on hydraulic conductivity K (m s^{-1}) and dynamic viscosity of the fluid μ (kg m^{-1} s^{-1}), porosity of the media ω_0, D_0 diffusion coefficient of a chemical species in free-water (m^2 s^{-1}), hydraulic head h (m) and elevation z (m). Considering an average argillite porosity of 7%, a water viscosity of 1.5×10^{-3} kg m^{-1} s^{-1}, a hydraulic gradient of 0.48 m m^{-1}, and an approximate D_0 for any elemental species dissolved in free-water equal to 5×10^{-9} m^2 s^{-1}, the Peclet number is equal to 1.7×10^{-11} for the highest hydraulic conductivity measured in the argillites where $K = 10^{-11}$ m s^{-1}.

[18] This Peclet number, which is greatly less than 1, describes mass transport essentially controlled by pure diffusion (at a large scale or locally). This means that if advection occurs, both advective mass transport and advective component of mass transport dispersion would be negligible. Therefore we assume that diffusion is the dominant process for migration of dissolved elements in pore water through these argillites [*Barescut and Michelot*, 1997; *Boisson et al.*, 1998b; *Bonin*, 1998; *Lavergne et al.*, 1997; *Moreau-Le Golvan*, 1997]. This assumption is the driving idea for establishing the protocol for extracting chloride (PECH protocol). This protocol yields assessment of chloride diffusion parameters (chloride concentrations and diffusion coefficients) using equilibration by diffusion within a cell, between chloride concentration in interstitial water of a rock sample and chloride concentration in initially chloride-free water. In order to reach our objectives, these experiments require that (1) measured chloride (in added water) only corresponds to the chloride contained in interstitial water and (2) measured chloride is really obtained by the diffusion process. In order to fulfill these two requirements, several laboratory analyses have been performed.

3. Characterizing the Various Reservoirs of Chloride

[19] Laboratory experiments performed in order to characterize the various reservoirs of chloride in the argillites were carried out on five samples (Table 1) from borehole VF4. In order to do so, each sample was divided in several aliquots (Figure 5).

3.1. Characterization of Argillites and Total Chloride Content

3.1.1. X-ray Diffractometry Analyses

[20] X-ray diffractometry analyses show the argillites consist of 30 to 40% of clay (Table 2), itself made up of 25% of illite, 10% of chlorite, 45% of kaolinite and 20% interstratified combinations of chlorite/illite or illite/smectite; clay compositions of the 5 samples are identical. Thus illite or illite/smectite constitutes at most 18% of the Tournemire material.

[21] Although no specific measurement of chemico-osmotic coefficients (reflecting efficiency of a material to behave as a membrane [see, e.g., *Malusis et al.*, 2001]) was performed, it seems improbable that Tournemire argillites are favorable for showing membrane capabilities that could affect further experiments and results. Indeed, *Malusis and Shackelford* [2002] worked on a sodium bentonite geosynthetic clay liner, extensively studied for its membrane properties by *Fritz and Marine* [1983], *Keijzer et al.* [1999], and *Kharaka and Berry* [1973]. This clay liner had a chemico-osmotic coefficient equal to 0.63, probably much higher than that of Tournemire argillites (a coefficient of 1 corresponds to an "ideal" membrane completely restricting

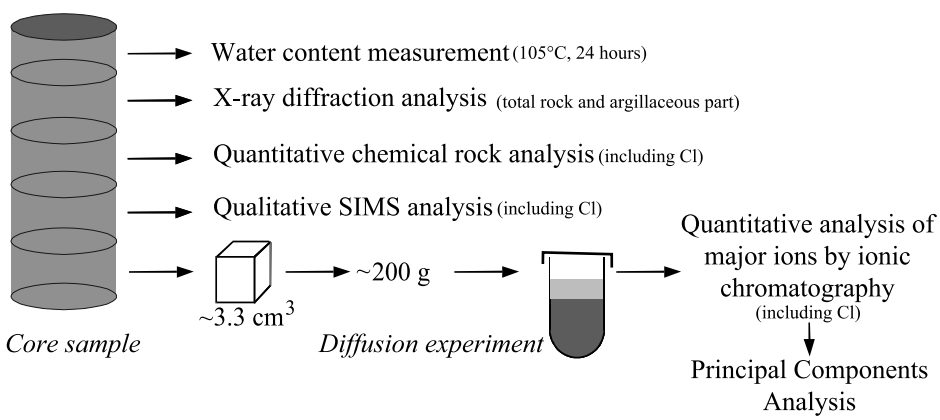

Figure 5. Analyses of five samples from borehole VF4: water content measurement, X-ray diffraction, chemical and SIMS analyses of the total rock, and diffusion experiments followed by ionic chromatographic analyses of water and principal component analysis on these data.

Table 2. Mineralogical Composition of VF4 Borehole Samples Obtained by X-ray Analysis

Sample	Clays, %	Quartz, %	Calcite, %	Dolomite, %	Others, %
VF4 06070	40	35	25	–	ε
VF4 06465	35	35	30	–	ε
VF4 06875	30	35	35	–	ε
VF4 07260	40	35	25	–	ε
VF4 07670	30	30	15	25	ε

the movement of electrolytes, and a value 0 corresponds to a material that exhibits no electrolyte restriction). They showed that, even with this high value of the chemico-osmotic coefficient, the diffusion coefficient increases by only 10%.

3.1.2. Quantitative Chemical Analyses on the Total Rock

[22] Major components of the rock were analyzed at the Centre de Recherches Pétrographiques et Géochimiques de Nancy, using the ICP AES (Atomic Emission Spectrometry with Inductively Coupled Plasma). Samples VF4 06070, VF4 06465, VF4 06875, and VF4 07260 have a very similar chemical composition; VF4 07670 contains more dolomite with higher concentrations of MgO, CaO, and CO_{2tot} (Table 3).

[23] Two analyses of the whole rock chloride content (including chloride in pore water) were performed at the CRPG (ICP AES) and a third was performed on VF4 06465 and VF4 06875 at the Wolff laboratory, using potentiometry (after combustion of the sample). Chloride concentrations for the three analyses range from 62 to 98 mg kg^{-1} (Table 3). While uncertainties of these values were not given, they are probably higher than 20%; indeed, an uncertainty of 20% is given by the CRPG for chloride concentrations higher than 5 g kg^{-1}. These high uncertainties make impossible to determine where chloride occurs in the rock. In order to get more accurate information about the chloride distribution, analyses were performed using SIMS.

3.2. Mapping Chloride in Argillites and Accessing to Chloride in Pore Water

3.2.1. SIMS Analyses

[24] Secondary ion mass spectrometry (SIMS) analysis is based upon the principle that a surface under ion bombardment (primary ions) emits charged particles (secondary ions) that can be analyzed for their mass (corresponding to the elements) with a mass spectrometer. The mass spectrometer determines the mass of a charged particle by accelerating the particle and then deflecting it with a magnetic field; low masses will be strongly deflected and high masses will be deflected less. The deflected particles pass through a slit to select a specific mass and can be detected using an electron multiplier (for measuring very low particle currents) or, in case of the secondary ion mass spectrometer, they can also be projected onto a channel plate resulting in a direct image of the elemental distribution at the sample surface. The spatial distribution of chloride, hydrogen, phosphorous, fluoride, oxygen, silica, sulfur, and carbon was obtained with SIMS (Cameca - Ims6f) analyses [*Raimbault*, 2000], using a 250 × 250 μm scanning (Figure 6).

[25] In a context of bulk chemical analyses (Table 3), samples appear to mainly consist of carbonate and clay with many grains of pyrite and some of apatite. Apatite is quite apparent in the VF4 07670 sample (Figure 6) where high concentrations of fluoride and phosphorus are coincident. High carbon concentrations reflect the presence of carbonate. Organic matter (reduced carbon not correlated with oxygen) is not recognized, probably because of very small grain sizes.

[26] SIMS analyses show that chloride is ubiquitous in all samples. Chloride concentrations correlate with hydrogen concentrations, indicating that chloride is in part associated with clayey phases. Correlation between chloride and carbon concentrations indicates that some chloride is probably present in carbonates. However, concentration of chloride in carbonates is not systematic.

Table 3. Chemical Analysis of Samples in SiO_2, Al_2O_3, Fe_2O_3, MnO, MgO, CaO, Na_2O, K_2O, TiO_2, and P_2O5 by ICP AES and in C_{org}, CO_{2tot}, and S_{tot} After Combustion Under Oxygen and in Cl^- for Analyses 1 and 2 by AAS After Alkaline Fusion

	Sample				
	VF4 06070	VF4 06465	VF4 06875	VF4 07260	VF4 07670
SiO_2, %	46.27	46.65	44.56	46.21	36.26
Al_2O_3, %	18.60	18.53	17.31	16.77	13.53
Fe_2O_3, %	5.21	4.85	5.18	5.02	6.60
MnO, %	0.03	<d.l.	0.04	0.03	0.08
MgO, %	1.86	1.81	1.88	1.76	4.50
CaO, %	8.18	8.27	10.62	10.26	14.21
Na_2O, %	0.28	0.29	0.30	0.30	0.25
K_2O, %	0.25	0.25	2.90	2.77	2.27
TiO_2, %	0.87	0.86	0.83	0.83	0.67
P_2O_5, %	0.25	0.22	0.25	0.20	0.20
Fire loss, %	15.19	15.21	16.53	15.70	21.88
Total, %	99.86	99.84	100.40	99.85	100.45
C_{org}, %	1.35	1.25	1.61	1.37	1.06
CO_{2tot}, %	11.58	11.15	14.58	13.38	20.39
S_{tot}, %	0.99	1.00	1.05	1.15	0.81
Cl^- analysis 1, mg kg^{-1}	78	80	80	87	69
Cl^- analysis 2, mg kg^{-1}	85	68	98	92	78
Cl^- analysis 3, mg kg^{-1}	–	62	82	–	–

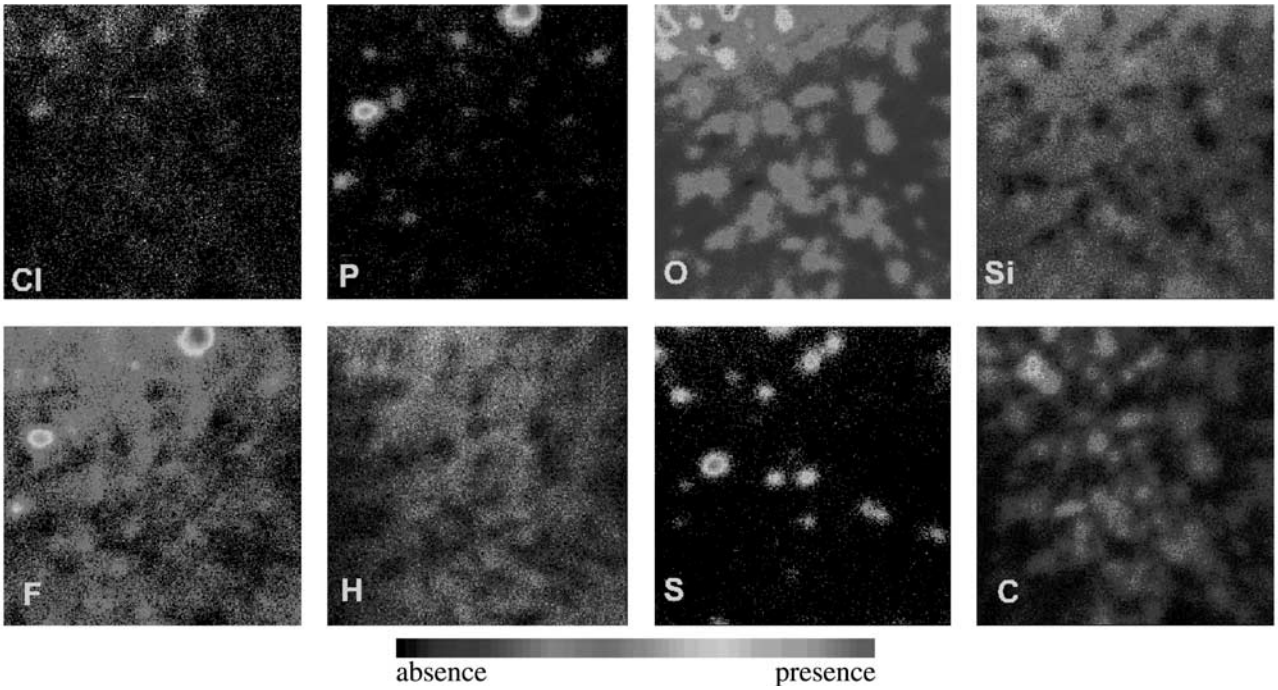

Figure 6. Distribution of chloride, phosphorus, fluoride, hydrogen, oxygen, silica, sulfur, and carbon obtained by SIMS analysis of sample VF4 07670 (sector D); 250 × 250 μm scan [*Raimbault*, 2000]. See color version of this figure at back of this issue.

[27] SIMS analysis of VF4 07670 shows that despite the ubiquitous presence of chloride in various minerals, there is a strong correlation between Cl, F, and P. This suggests that some minerals, like apatite, contain chlorine in high quantity. Chloride content in apatites was estimated to be about 14% of the total chloride content of the rock.

3.2.2. Preliminary Diffusion Experiments

3.2.2.1. Experimental Settings for the Preliminary Diffusion Experiments and Data Collection

[28] Diffusion experiments were performed on pieces of rock cut into cubes with an approximate volume of 3.3 cm^3 each and an approximate total weight of 200 g. For each rock sample, the cubes were placed in a Teflon® container. Ultra-pure water was added until rock/water ratio around 2270 g L^{-1} was attained (approximately 88 mL).

[29] Diffusion of chloride from the sample pore water to the added water was monitored by chromatographic analysis of several successive water samples; anions (fluoride, chloride, nitrite, bromide, nitrate, sulfate) and cations (lithium, sodium, ammonium, potassium, magnesium, calcium) were measured.

[30] For each of the five samples, at least 12 water samples were collected during the 35 weeks of diffusion experiments. Expecting a very low diffusion coefficient, the sampling was planned for after 1, 2, 4, 6, 8, 11, 14, 17, 20, 24, 28, 31 and 35 weeks of diffusion. For most analyses, bromide content was below the detection limit. This data set constitutes a sum of more than 660 analyses (see data of *Patriarche* [2001]).

3.2.2.2. Principal Component Analysis of Chemical Data From Preliminary Diffusion Experiments

[31] A principal component analysis (PCA) was used to extract information from this data set. The method is widely used in signal processing, statistics, and neural computing and is based on the concept of finding the components f_1, f_2,... f_n so that they explain the maximum amount of variance possible by *n* linearly transformed components [see, e.g., *Dazy et al.*, 1996; *Jolliffe*, 1986]. PCA expresses several variables as a set of linear combinations of noncorrelated components. This method allows for the representation of primary data (statistical units corresponding to the data in this study) in a space with a lower dimension than the primary space, limiting the loss of information. PCA is useful for summarizing data described by several quantitative variables, and for obtaining noncorrelated factors.

[32] Principal component analysis of corrected chemical data (expressed as mg kg^{-1} of rock) shows the particular behavior of chloride in comparison with the other elements. The circle of the intervariable correlations (Figure 7) generated by PCA allows for the identification of two main processes during the experiments: (1) The strong correlation between potassium, magnesium, sodium, sulfate, calcium and time reflects the alteration of argillaceous minerals. However, the strong colinearity between the vector of factor 1 and the calcium can be explained by the dissolution of calcite. In the same way, the strong colinearity between the vector of factor 1 and sulfate reflects the dissolution of pyrite. This process is strongly linked to time. Consequently, factor 1, which explains 65% of the variance for the data represents minerals alteration processes. (2) In contrast to factor 1, the factor 2 (13% of the variance) is essentially expressed by chloride variation, and is not significantly correlated with any other variable. This shows that in the diffusion experiments, chloride concentration is not linearly correlated with any other chemical species, or with time. The nonlinear nature of the relationship between time and chloride concentration suggests that chloride migrates in water by diffusion. The behavior of some species (with very

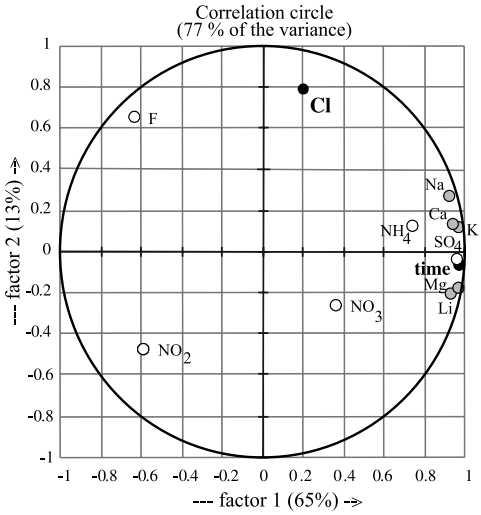

Figure 7. Space of the variables of the principal component analysis performed on chemical data obtained during diffusion experiments done for elaborating the protocol for extracting chloride; variables include major anions and cations and time. The first factor expressing 65% of the variance represents the alteration of minerals. The second factor expresses the diffusion process (no linear correlation with time). The good correlation between chloride and factor 2 suggests that chloride is essentially controlled by diffusion.

low correlations according to the first and second factors) such as NO_2 and NO_3, may be explained by other processes. Indeed, oxidoreduction, precipitation, etc. could have a role on the rest of the variance.

[33] Moreover, noncorrelation between chloride and calcium (r = 0.35; Table 4) shows that calcite dissolution during maceration experiments did not release fluid inclusions highly charged in chloride. This observation suggests that, in these five samples, chloride does not strongly occur in calcite. As a conclusion, principal component analysis strongly suggests that chloride measured during these experiments is in large part derived by diffusion from interstitial water.

3.2.3. Diffusion Experiments on Crushed Samples and Concluding Remarks

[34] Additional diffusion experiments were performed on crushed samples with various granulometry sizes ranging from 0 to 20 mm. The fraction containing the material sized from 0 mm to 0.4 mm is called the fraction F. The chloride extracted (mg kg^{-1}_{rock}) during these additional experiments and that extracted during the preliminary diffusion experiments is obtained by

$$C_{ppm\_from\_rock} = 10^3 \frac{C_{mg.l^{-1}}}{\frac{R}{W_{final}}},$$

with $C_{mg\ l^{-1}}$ the final chloride concentration of the added water (mg L^{-1}) at the steady state of diffusion, R the initial rock mass (g) considered constant over the successive water samplings, W_{final} the final volume of water added (L) obtained by $W_{final} = W_{initial} - s\ V_{water\ sampling}$ after the last sth water sampling (L).

[35] Values of extracted chloride content for the (cubes) diffusion experiments and for the fraction F (Table 5 and Figure 8) as well as total chlorine concentration of each rock sample before chloride extraction, suggest that efficiencies of the diffusion experiments are between 5% and 7.1%. These results are very homogeneous for all samples.

[36] For crushed samples of various granulometry sizes, results were very similar to those obtained for the (cubes) diffusion experiments except for the F fractions. Indeed, in two out of five samples, chloride extraction efficiency for the finely crushed samples is higher for cubes or for samples with lower granulometry sizes. It means that chloride can be located (1) in some pores enclosing water with concentrated chloride, (2) in the vicinity of cation compensation sites, near argillaceous layers, and (3) in some minerals. For these three reservoirs of chloride, the chloride would stay trapped unless the reservoir itself was crushed or dissolved.

[37] For the ''minerals'' reservoir, the SIMS analysis reveals that, despite of a rather ubiquitous distribution of chlorine throughout the matrix of all samples, chloride could be strongly concentrated in grains of apatite; however, this would represent only 14% of the total chloride content of the rock. SIMS analyses also reveal that chloride is present in some carbonates, but its presence is not systematic; quantitative assessment of this reservoir was not possible. Thus the very low efficiencies of diffusion experiments can be explained considering that most chlorine is fixed into minerals, and only the dis-

Table 4. Matrix of Intervariables Correlations From Principal Component Analysis on Chemical Data of Diffusion Experiments

	Time	F	Cl	NO_2	NO_3	SO_4	Li	Na	NH_4	K	Mg	Ca
Time	1.00											
F	−0.66	1.00										
Cl	0.14	0.28	1.00									
NO_2	−0.59	0.09	−0.26	1.00								
NO_3	0.44	−0.43	0.14	−0.12	1.00							
SO_4	0.94	−0.60	0.16	−0.48	0.27	1.00						
Li	0.89	−0.66	0.01	−0.39	0.32	0.93	1.00					
Na	0.87	−0.45	0.31	−0.72	0.32	0.82	0.75	1.00				
NH_4	0.66	−0.36	0.04	−0.39	−0.20	0.75	0.73	0.73	1.00			
K	0.89	−0.52	0.23	−0.60	0.29	0.90	0.85	0.96	0.80	1.00		
Mg	0.93	−0.70	0.00	−0.48	0.33	0.93	0.89	0.82	0.72	0.90	1.00	
Ca	0.89	−0.51	0.35	−0.51	0.36	0.89	0.79	0.87	0.66	0.89	0.86	1.00

Table 5. Experiment Efficiencies for Chloride Extraction by the Diffusion Experiments (Diffu Using PECH) and for Fractions F

	VF4 06070		VF4 06465		VF4 06875		VF4 07260		VF4 07670	
	F	Diffu	F	Diffu	F	Diffu	F	Diffu	F	Diffu
$[Cl]_{tot}$ average, mg kg^{-1}	82	82	70	70	87	87	90	90	74	74
Extracted Cl, mg kg^{-1}	5.7	4.9	12.4	5.0	4.0	4.8	9.0	5.0	3.4	3.7
Uncertainty, mg kg^{-1}	0.3	0.4	0.3	0.4	0.3	0.4	0.4	0.4	0.4	0.4
Experiment efficiency, %	6.9	6.0	16.7	7.1	4.4	5.5	10.0	5.6	4.7	5.0

solved chloride is able to diffuse. Principal component analysis shows that the amount of chloride derived by mineral dissolution is small, as is that coming from fluid inclusions in carbonates. Thus despite low extraction efficiencies, it appears that the (cubes) diffusion experiments using distilled water allow for an assessment of chloride that is able to diffuse from (or in) interstitial water.

4. Protocol for Extraction of Chloride: Measuring the Chloride Concentration in the Pore Water and Determining the Chloride Diffusion Coefficients

4.1. Principle

[38] Laboratory experiments show that equilibration between chloride concentration in interstitial water and chloride concentration in initially chloride-free water, allows for an assessment of the initial chloride concentration in interstitial water utilizing the diffusion process. We can model the diffusion experiments using Fick's second law coupled to mass conservation law, which expresses the equality between the rate of mass change in a volume (having a porosity) and an instantaneous balance of the solute entering and leaving some element. The chloride diffusion coefficient and the initial concentration can be determined using this model.

4.2. Experimental Settings of Diffusion Experiments for the PECH

4.2.1. Contribution of the Preliminary Laboratory Works

[39] Chloride concentrations measured in added water during preliminary diffusion (Figure 9) on five samples from borehole VF4 (Table 1) show that the transient part of diffusion is not well described; too few data are collected using the sequence described in section 3.2.2. These do not allow for confident determination of the chloride diffusion coefficient. In order to evaluate this parameter, sampling has to be greater over the first two weeks of the experiments.

[40] Figure 9 shows an unexpected chloride behavior. After a few weeks of diffusion, one would expect a constant concentration reflecting steady state of diffusion; instead, chloride concentration oscillates. This behavior is not readily explained. A stepped increase in chloride concentration could reflect access to various pores during mineral dissolution. However, the decrease of the chloride concentration remains unexplained if this dissolution process is the cause of the increase of chloride concentration. Moreover, the study of the cation and anion behavior did not permit to find

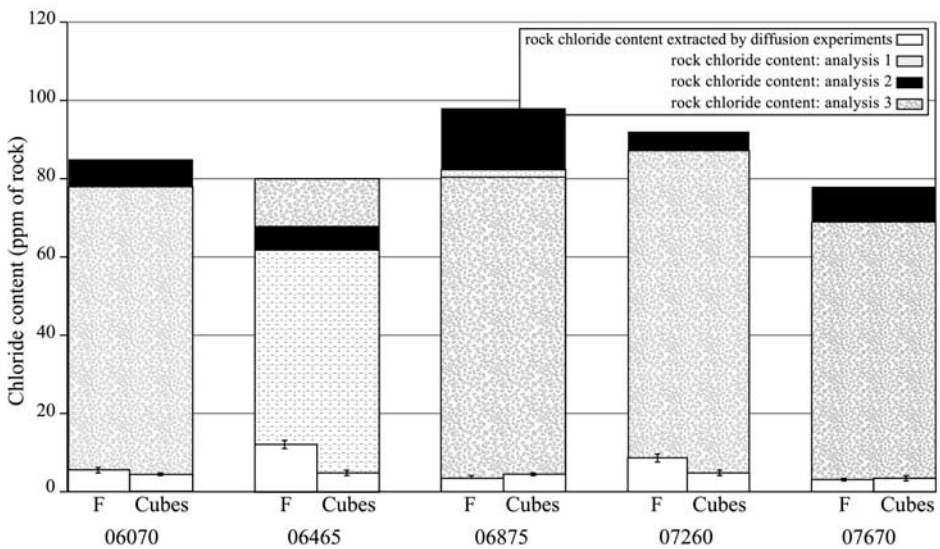

Figure 8. Comparison for each sample between the chloride contents of the rock (expressed as mg per kg of rock) before the (preliminary) diffusion experiments (analyses 1, 2, and 3) and extracted by the diffusion experiments on the cubes and the fraction F where grain size <0.4 mm. Less than 10% of the chloride is extracted, meaning that the main part of chloride is trapped in the minerals or nonconnected pores. This is confirmed by the highest chloride content extracted on crushed materials (fraction F).

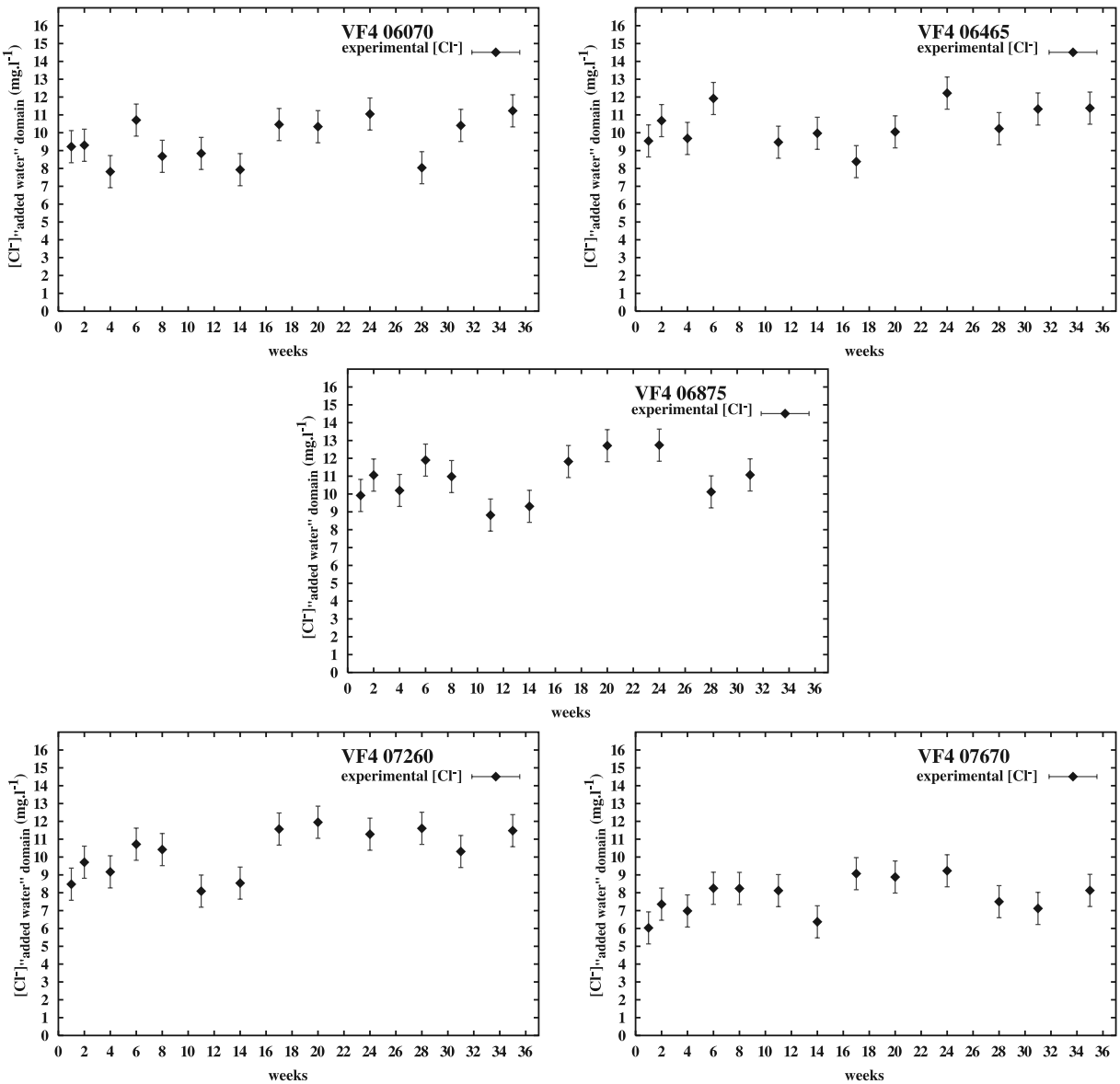

Figure 9. Chloride concentration (precision of measurement is ±9.5%) over time for the preliminary diffusion experiments for the five studied samples coming from borehole VF4. There is lack of data for a good representation of the transient state for the diffusion process and unexpected behavior (decrease/increase) of chloride concentration over the "steady state."

a chemical process for explaining this unexpected behavior of chloride. On the one hand, no mineral containing chloride is able to precipitate at the very low chloride concentrations measured; the solution is largely under chloride saturated. On the other hand, the readsorption of chloride to the surface of clays seems unlikely; *Nolin* [1997] has shown the nonadsorption of the main part of anions and especially chloride, on the surface of clays in natural water, and *Fletcher and Sposito* [1989] have shown anion adsorption on the surface of clays only when these anions form complexes with divalent cations. Unexpected behavior of chloride is not specific to this study; *van der Kamp et al.* [1996] do not have explanations for the discrepancies for the results obtained for chloride using their radial diffusion method. Thus this behavior of chloride is still not understood, and seems to be related more to a physical process than to a chemical one; but obviously, it is corresponding to another process than diffusion, and may explain that, in the PCA of the preliminary diffusion experiments, the chloride variable is not perfectly located on the circle of intervariable correlation (Figure 7).

4.2.2. Settings of the Diffusion Experiments of the PECH Protocol

[41] For the diffusion experiments of the PECH protocol, the samples were prepared in the same way as for the preliminary experiments.

4.2.2.1. Preparation and Storage of Samples

[42] Each sample from a core of argillite obtained by cutting cubes with an approximate volume of 3.3 cm^3 each (~1.5 cm on a side); each face of the cube was either perpendicular or parallel to stratification. The cubes (~200 g) were placed in a 400 mL Teflon® reservoir that had been rinsed several times with ultra-pure water. The reservoir was weighted before and after introducing the rock

sample; the exact weight of the rock sample was determined. Ultra-pure water was added in the reservoir, the reservoir was reweighted, and the exact weight (and volume) of water was determined, and the rock/water (R/W) ratio was calculated. R/W ranged between 1884 and 3008 g L^{-1}. These rock/water ratios were quite high because at high rock/water ratio, a variation of this ratio generates a low variation of the amount of extracted chloride [*Moreau-Le Golvan*, 1997]; and so, it allows for the comparison between experiments with different rock/water ratios.

[43] In order to preclude bacteria activity, diffusion reservoirs were kept under ultraviolet light (254 nm) during the equilibration experiments. A screwing cap was placed on the top of the reservoir to avoid evaporation. Reservoirs were stored between 12° and 18°C.

4.2.2.2. Sampling Sequence and Chemical Analyses

[44] Diffusion for the PECH experiments was monitored over 30 days, and sampling was planned in order to cover both transient and steady state of diffusion. Samplings (1 mL removed at a time) occurred at 5, 12, 24, 40, 62, 120, 238, 543, 975, and 1750 hours after the water was added into the reservoirs. Anions and cations (fluoride, chloride, nitrite, bromide, nitrate, sulfate and lithium, sodium, ammonium, potassium, magnesium, calcium) were measured by liquid chromatographic analysis (data of *Patriarche* [2001]).

4.3. Numerical Modeling of Diffusion Experiments and Parameters

[45] The numerical simulations were performed using the code METIS, a finite element program developed by the Centre d'Informatique Géologique of the Ecole des Mines de Paris [*Cordier and Goblet*, 1999; *Goblet*, 1989].

[46] In our case, only pure diffusion transport is simulated, and METIS resolves the equation $div\left(\omega_d \overline{\overline{D_p}} \overrightarrow{grad} C\right) = \omega_d \frac{\partial C}{\partial t}$ expressing Fick's second law, where $\overline{\overline{D_p}}$ is the tensor of the pore diffusion coefficient ($m^2\ s^{-1}$) of some chemical species in the porous media, ω_d is the diffusion porosity of the chemical species (here taken as equal to the geochemical porosity ω_{geoch}) and where C is the concentration of the species in water.

4.3.1. Physical Properties of the Argillites: Parameters for the Model

4.3.1.1. Porosity

[47] The geochemical porosity ω_{geoch} is the porosity occupied by some dissolved chemical species in the water. It is lower than total porosity, because some nonconnected pores and pores that are too small (e.g., anion exclusion process in clays) do not participate in geochemical porosity. *Pearson* [1999] lists several values for geochemical porosities for various chemical species and various rocks. In our study, total porosity ω_t is considered as being equal to the porosity ω_0 obtained from water content; the ratio $\frac{\omega_{geoch}}{\omega_t}$ has been called the Pearson coefficient and a value $\frac{\omega_{geoch}}{\omega_0} \approx 0.3$ has been adopted. This value corresponds to the value of the ratio $\frac{\omega_{geoch}}{\omega_t}$ given by *Pearson* [1999] for chloride in Parlfris marl (where water content, like in Tournemire marls and argillites, is equal to about 3%).

4.3.1.2. Diffusion Coefficient and Anisotropy

[48] A three dimensional representation of the diffusion experiment (section 4.3.2) allows for use of different diffusion coefficients in three dimensions of space. *Beaudoing et al.* [1996] performed diffusion-permeation experiments of tritiated water on 14 core samples from the ID boreholes. Ten were collected on the vertical ID 0 and ID 180 boreholes (i.e., near-perpendicular to bedding), including one in the Domerian, one in the Lower Toarcian, one in the Middle Toarcian, and seven in the Upper Toarcian. The four others were collected on the horizontal ID 90 and ID 270 boreholes (i.e., near-parallel to bedding) at the tunnel level. Results [*Beaudoing et al.*, 1996] for diffusion coefficient values for tritiated water between these two series are 2 to 3 times different. To the best of our knowledge, anisotropy of diffusion coefficients in clayey sedimentary materials is not extensively described in the literature. However, anisotropy for diffusion coefficients in Tournemire material is very similar to that of the Boom Clay in Belgium [*Maes et al.*, 1999; *Put et al.*, 1991], and can be explained by the structure of the material (phyllosillicates which can be represented by a pore model with parallel linings [*Boisson et al.*, 1998c]). Thus, in order to take into account the high anisotropy of the system (anisotropy 1:2), the diffusion coefficients were determined by a three dimensional model of the diffusion experiments, according to $D_x = D_y = 2D_z$. Despite the lack of diffusion coefficient values in the horizontal direction in the lower part of the sequence, we ascribe the same anisotropy value for the diffusion coefficients to the lower layers because they also present a very stratified structure.

4.3.1.3. Pore Diffusion Coefficient and Effective Diffusion Coefficient

[49] As described previously, the equation solved by METIS uses the porosity in the two members of the equation and the pore diffusion coefficient D_p, which expresses the rate extension of the diffusion front in the poral space; tortuosity of the poral space is therefore taken into account. The equation solved by METIS is exactly equivalent to $div\left(\overline{\overline{D_e}} \overrightarrow{grad} C\right) = \omega_{geoch} \frac{\partial C}{\partial t}$, which expresses the rate extension of the diffusion front in the porous media and where D_e is the effective diffusion coefficient and ω_{geoch} is the geochemical porosity of the media for the considered species; D_e takes into account both tortuosity and porosity of the media. Thus D_e is the diffusion coefficient used to compare mass fluxes between various tracers (part 2 of this study [*Patriarche et al.*, 2004]). Nonetheless, diffusion coefficients rendered by METIS are pore diffusion coefficients, and all following results are expressed as D_p. Conversion from one to another is given by $\overline{\overline{D_e}} = \omega_{geoch} \overline{\overline{D_p}}$ knowing ω_{geoch}. Finally, in the model, $\overline{\overline{D_p}}$ is expressed as

$$\overline{\overline{D_p}} = \begin{pmatrix} D_p & 0 & 0 \\ 0 & D_p & 0 \\ 0 & 0 & \frac{D_p}{2} \end{pmatrix}$$

reflecting the 1:2 anisotropy of the system.

4.3.2. Representation of the Diffusion Experiments

4.3.2.1. Rock Sample, Added Water and Geometrical Representation

[50] Diffusion experiments were simulated with a three dimensional model. Instead of several cubes used during the diffusion experiments, the model consists only of one cube, in a larger cube of water reflecting the rock/water ratio of the experiment (Figure 10a). This approximation

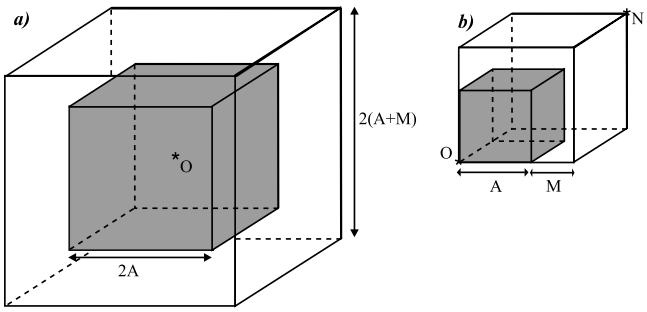

Figure 10. (a) Geometrical representation used in the finite element model of diffusion experiments and (b) one eighth of this representation used for calculations.

of the experiment can be done because the diffusion coefficient of chloride in the added water is initially about two orders of magnitude higher than that in the rock (considering the rock porosity), and so instantaneous homogenization can be assumed in the surrounding water. Moreover, equilibration rate in the experiment is controlled by surface area between the cube and surrounding water, and the concentration gradient between the two domains. The cubic representation of this model reflects the volume and surface proportions of the real system. The regular shape of the cubic model allows for calculation of the mesh used in numerical simulations. In order to limit time calculation, we represent one eighth of the domain (Figure 10b). The geometrical representation used for building the mesh is determined for each sample (each diffusion experiment) as:

[51] A is the $^1/_2$ length of the ridge (2A = 1.5 cm) of the rock cube. The rock mass (g) is $R = d^*(2A)^3$, with d being the rock density equal to 2500 g L^{-1}. The volume of surrounding water is $W = (2(M + A))^3 - (2A)^3$. The rock/water ratio (g L^{-1}) is $\frac{R}{W} = \frac{d(2\mathrm{A})^3}{(2(\mathrm{M}+\mathrm{A}))^3 - (2\mathrm{A})^3}$. Thus M is $A\left(\sqrt[3]{\frac{d}{R/W}+1}-1\right)$.

4.3.2.2. Mesh Features and Simulation of the Decrease of the Water Volume After Each Water Sampling

[52] In order to guarantee the correct convergence of the calculations, especially at the boundaries between rock and "added water" domains, the mesh was extremely refined because at these boundaries strong contrasts of porosity and diffusion coefficient occurred; the mesh was constituted by 15625 nodes and 13824 cubic cells.

[53] After each water sampling, the R/W ratio was recalculated (R is constant). To account for the decrease of the water volume, porosity of the "added water" domain (initially 100%) was decreased according to the new R/W. The calculation applied to the next sampling and the R/W was reevaluated. The new porosity corresponding to the new rock/water ratio is given by

$$\omega_{\text{"addedwater" domain}} = \left(\left(\frac{(R/W)_{initial}}{(R/W)_{new}}\right)^*\left((\mathrm{M}+\mathrm{A})^3 - \mathrm{A}^3\right) + \mathrm{A}^3\right) {}^*(\mathrm{M}+\mathrm{A})^{-3}.$$

[54] Decrease in R/W did not have a great impact on calculations. For instance, the diffusion experiment for the sample TN3 02020 used 181.29 g of rock and initially 77.69 mL of ultra-pure water (R/W = 2333.50 g L^{-1}). After 10 samplings, the final volume of water is 67.69 mL and the rock/water ratio is R/W = 2678 g L^{-1}. The equivalent porosity of the "added water" at the final rock/water ratio was 95.9%.

4.3.3. Determination of Chloride Concentration and Chloride Diffusion Coefficients

4.3.3.1. Imposed Conditions for the Diffusion Model

[55] The initial concentration of chloride in added water is equal to 0 mg L^{-1} and the isotropic chloride diffusion coefficient in "added water" was assumed to be 17.1×10^{-10} m^2 s^{-1}, the value in pure water at 18°C [*Li and Gregory*, 1974]; this is an approximation because as the diffusion occurs, water is no longer ultra-pure.

[56] For each rock sample, porosity corresponded to the geochemical porosity for chloride, obtained initially by the calculation of total porosity from water content measurement. As described previously (section 4.3.1), the geochemical porosity assigned to argillites equals $0.3\omega_\theta$. For the samples collected in the Aalenian (limestone), the geochemical porosity equals ω_θ (the total porosity obtained from water content). An initial concentration of chloride was set for all simulations, and the pore diffusion coefficient was also chosen. These two parameters are the variables we want to determine from simulations; they are obtained by trial and error.

4.3.3.2. Fitting the Model to Experimental Data

[57] At the end of a simulation, calculated concentrations at the node farthest of the rock (point N on Figure 10b) and at the center of the cube of rock (point O on Figure 10b) are extracted and plotted over time. Results of diffusion experiments on various samples (Figure 11) shows that chloride concentrations increase rapidly at the node in the "added water" (point N) and then tend to remain constant. Theoretically, steady state is never reached, but practically, we considered it as reached when difference between chloride concentrations in the center of the cube and in the "added water" domain is less than the analytical uncertainty $\Delta C_{measured}$.

[58] For fitting the model to experimental data, two criteria were used. For each rock sample, we maximized the number of experimental data (n) out of t data where $|C_{measured} - C_{calculated}| \leq \Delta C_{measured}$ is satisfied. For the same simulation, once n was maximized, we minimized S, the weighted sum of the square differences given by $\frac{1}{t}\sum_1^t (C_{measured} - C_{calculated})^2$.

[59] Theoretically, in the case of a perfect mixing between chloride of interstitial water and chloride of added water (initially zero), the final concentration in the "added water" domain would not depend on the chloride diffusion coefficient and would only depend on the initial concentrations and initial volumes of water in the two domains. In practice, we did notice that sometimes the final model concentration did not allow minimizing the criterion n (due to the unexplained chemical behavior of the chloride described section 4.2.1). This was not generally the case.

[60] Practically, we minimized n and then S, only with respect to steady state diffusion. Once initial concentration was found, we used the same trial-and-error method to determine the chloride pore diffusion coefficient, by minimizing n and then S over the transient part of the

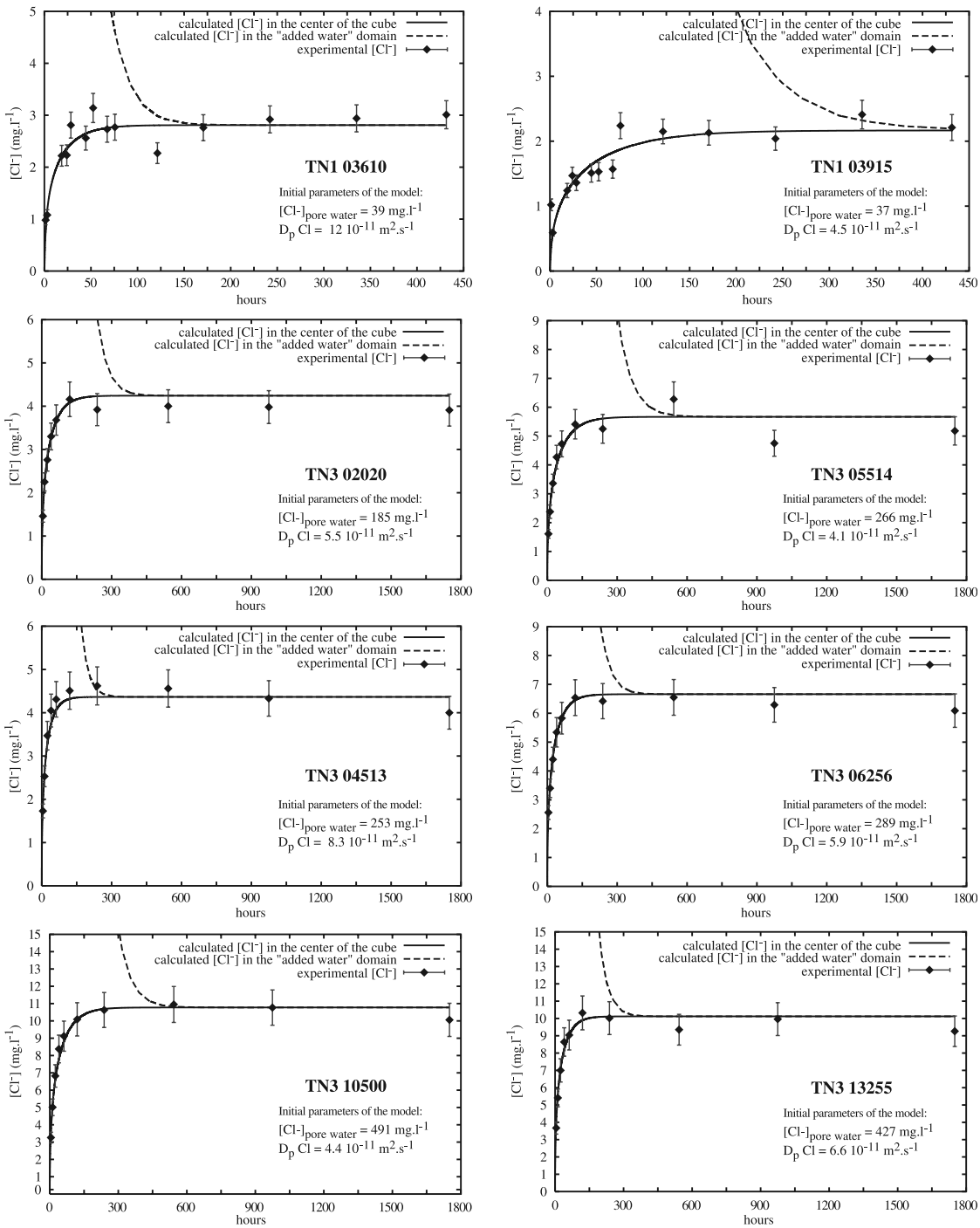

Figure 11. Diffusion experiments for samples from boreholes TN1 and TN3 calibrated by a trial-and-error method, yielding the chloride diffusion coefficient (calibrated on transient state) and the pore water chloride concentration (calibrated on steady state).

diffusion. Once the two parameters were set, we checked that estimation of the a priori steady state part was indeed an a posteriori steady state. If it was not, we restarted the whole process with the most recently defined diffusion coefficient.

4.4. Accuracy of the Results

[61] Because of the low number of water samples collecting during each experiment and due to the fact that porosity was derived only using the water content, we were unable to calculate the uncertainties on pore water chloride concentrations or chloride diffusion coefficients. However, when simulations are repeated using a ±0.3% variation in water content; the average variation for the interstitial water chloride concentration is ∓10%. Moreover, variation in water content has no impact on the value of the diffusion coefficient because the pore diffusion coefficient merely reflects dynamics of the system in reproducing experimental

Table 6. Sample, Elevation, Elevation Corrected From Stratigraphy (Boreholes TN1 and TN3 Chosen as the Reference), Water Content, Porosity Calculated From Water Content, Geochemical Porosity for Chloride, Rock/Water Ratio of the Corresponding Diffusion Experiment, Number of Experimental Data Reproduced by the Model Versus Number of Available Experimental Data, Pore Diffusion Coefficient for Chloride, Effective Diffusion Coefficient for Chloride and Chloride Concentration of Interstitial Water[a]

Sample	Elevation, m	Corrected Elevation, m	θ, %	$\omega_{\theta,}$ %	$\omega_{geoch,}$ %	R/W, g L^{-1}	Data mod/exp	D_p, m^2 s^{-1}	D_e, m^2 s^{-1}	$[Cl^-]_{I.W.}$, mg L^{-1}
TN1 00600	531.2	531.2	3.60	9.0	2.7	2241	7/14	**4.40×10^{-11}**	1.19×10^{-12}	**99**
TN1 00700	532.2	532.2	2.61	6.5	2.0	2766	2/3	4.73×10^{-11}	9.27×10^{-13}	**163**
TN1 00800	533.2	533.2	4.02	10.1	3.0	2494	2/3	5.07×10^{-11}	1.53×10^{-12}	**67**
TN1 00900	534.2	534.2	3.89	9.7	2.9	2748	3/3	5.40×10^{-11}	1.58×10^{-12}	**73**
TN1 00992	535.1	535.1	3.10	7.8	2.3	2698	1/3	5.71×10^{-11}	1.33×10^{-12}	**86**
TN1 01100	536.2	536.2	3.46	8.7	2.6	2371	1/3	6.07×10^{-11}	1.57×10^{-12}	**134**
TN1 01200	537.2	537.2	3.14	7.9	2.4	2017	6/14	**6.40×10^{-11}**	1.51×10^{-12}	**119**
TN1 01300	538.2	538.2	3.20	8.0	2.4	2559	1/3	6.73×10^{-11}	1.61×10^{-12}	**156**
TN1 01400	539.2	539.2	2.37	5.9	1.8	2726	2/3	7.06×10^{-11}	1.25×10^{-12}	**147**
TN1 01500	540.2	540.2	2.90	7.3	2.2	2018	2/3	7.39×10^{-11}	1.61×10^{-12}	**112**
TN1 01594	541.1	541.1	3.71	9.3	2.8	2614	2/3	7.69×10^{-11}	2.14×10^{-12}	**59**
TN1 01695	542.1	542.1	2.71	6.8	2.0	2937	1/3	8.03×10^{-11}	1.63×10^{-12}	**88**
TN1 01790	543.1	543.1	3.60	9.0	2.7	2710	2/3	8.34×10^{-11}	2.25×10^{-12}	**67**
TN1 01900	544.2	544.2	2.64	6.6	2.0	2022	7/14	**8.70×10^{-11}**	1.72×10^{-12}	**71**
TN1 02000	545.2	545.2	2.00	5.0	1.5	2739	1/3	8.70×10^{-11}	1.31×10^{-12}	**148**
TN1 02100	546.2	546.2	3.87	9.7	2.9	2391	1/3	8.70×10^{-11}	2.53×10^{-12}	**117**
TN1 02205	547.2	547.2	3.83	9.6	2.9	2438	1/3	8.70×10^{-11}	2.50×10^{-12}	**135**
TN1 02280	548.0	548.0	2.14	5.4	1.6	2238	1/3	8.70×10^{-11}	1.40×10^{-12}	**168**
TN1 02390	549.1	549.1	3.85	9.6	2.9	2443	2/3	8.70×10^{-11}	2.51×10^{-12}	**67**
TN1 02485	550.0	550.0	4.05	10.1	3.0	2318	8/14	**8.70×10^{-11}**	2.64×10^{-12}	**34**
TN1 02600	551.2	551.2	4.32	10.8	3.2	2370	1/3	7.58×10^{-11}	2.46×10^{-12}	**57**
TN1 02705	552.2	552.2	4.02	10.1	3.0	2621	3/3	6.56×10^{-11}	1.98×10^{-12}	**52**
TN1 02795	553.1	553.1	3.99	10.0	3.0	2631	1/3	5.69×10^{-11}	1.70×10^{-12}	**56**
TN1 02855	553.7	553.7	3.87	9.7	2.9	2572	1/3	5.10×10^{-11}	1.48×10^{-12}	**72**
TN1 02900	554.2	554.2	4.50	11.3	3.4	2508	1/3	4.66×10^{-11}	1.57×10^{-12}	**58**
TN1 02958	554.8	554.8	4.50	11.3	3.4	2444	6/14	**4.10×10^{-11}**	1.38×10^{-12}	**53**
TN1 02990	555.1	555.1	1.84	4.6	1.4	2599	1/3	4.05×10^{-11}	5.60×10^{-13}	**138**
TN1 03030	555.5	555.5	3.64	9.1	2.7	2543	1/3	4.00×10^{-11}	1.09×10^{-12}	**130**
TN1 03118	556.4	556.4	4.40	11.0	3.3	2701	1/3	3.87×10^{-11}	1.28×10^{-12}	**95**
TN1 03190	557.1	557.1	3.37	8.4	2.5	2529	1/3	3.77×10^{-11}	9.53×10^{-13}	**64**
TN1 03250	557.7	557.7	5.03	12.6	12.6	2619	2/3	3.69×10^{-11}	4.63×10^{-12}	**13**
TN1 03310	558.3	558.3	3.95	9.9	9.9	2426	4/14	**3.60×10^{-11}**	3.56×10^{-12}	**12**
TN1 03385	559.0	559.0	1.12	2.8	2.8	2294	3/3	5.70×10^{-11}	1.60×10^{-12}	**132**
TN1 03440	559.6	559.6	2.16	5.4	5.4	2371	2/3	7.24×10^{-11}	3.91×10^{-12}	**51**
TN1 03499	560.2	560.2	2.11	5.3	5.3	2467	2/3	8.89×10^{-11}	4.69×10^{-12}	**60**
TN1 03559	560.8	560.8	2.00	5.0	5.0	2316	2/3	1.06×10^{-10}	5.29×10^{-12}	**63**
TN1 03610	561.3	561.3	3.11	7.8	7.8	2470	10/14	**1.20×10^{-10}**	9.33×10^{-12}	**39**
TN1 03670	561.9	561.9	1.07	2.7	2.7	2540	2/3	1.05×10^{-10}	2.82×10^{-12}	**141**
TN1 03730	562.5	562.5	1.45	3.6	3.6	2714	3/3	9.05×10^{-11}	3.28×10^{-12}	**121**
TN1 03785	563.0	563.0	2.36	5.9	5.9	2933	0/3	7.70×10^{-11}	4.54×10^{-12}	**30**
TN1 03845	563.6	563.6	3.60	9.0	9.0	2613	1/3	6.22×10^{-11}	5.60×10^{-12}	**28**
TN1 03915	564.3	564.3	2.88	7.2	7.2	2121	9/14	**4.50×10^{-11}**	3.24×10^{-12}	**37**
TN1 03970	564.9	564.9	2.37	5.9	5.9	2331	1/3	4.30×10^{-11}	2.55×10^{-12}	**38**
TN1 04040	565.6	565.6	1.06	2.7	2.7	2308	1/3	4.04×10^{-11}	1.07×10^{-12}	**80**
TN1 04115	566.3	566.3	1.51	3.8	3.8	2766	2/3	3.77×10^{-11}	1.42×10^{-12}	**107**
TN1 04180	567.0	567.0	0.87	2.2	2.2	2010	2/3	3.54×10^{-11}	7.69×10^{-13}	**119**
TN1 04272	567.9	567.9	1.80	4.5	4.5	3008	6/14	**3.20×10^{-11}**	1.44×10^{-12}	**80**
TN1 04340	568.6	568.6	2.20	5.5	5.5	2385	2/3	3.57×10^{-11}	1.96×10^{-12}	**81**
TN1 04400	569.2	569.2	1.43	3.6	3.6	2997	3/3	3.89×10^{-11}	1.39×10^{-12}	**63**
TN1 04455	569.7	569.7	1.47	3.7	3.7	2553	2/3	4.18×10^{-11}	1.54×10^{-12}	**115**
TN1 04540	570.6	570.6	0.95	2.4	2.4	2194	3/3	4.64×10^{-11}	1.10×10^{-12}	**138**
TN1 04607	571.2	571.2	0.95	2.4	2.4	2372	10/14	**5.00×10^{-11}**	1.19×10^{-12}	**116**
TN3 00969	509.9	509.9	3.6	9.0	2.7	2534	7/10	**5.20×10^{-11}**	1.40×10^{-12}	**135**
TN3 01500	504.5	504.5	3.4	8.5	2.6	1884	8/10	**5.20×10^{-11}**	1.33×10^{-12}	**167**
TN3 02020	499.3	499.3	3.3	8.3	2.5	2334	10/10	**5.50×10^{-11}**	1.36×10^{-12}	**185**
TN3 02520	494.3	494.3	3.3	8.3	2.5	1907	9/10	**4.90×10^{-11}**	1.21×10^{-12}	**156**
TN3 03010	489.4	489.4	3.3	8.3	2.5	2426	9/10	**4.60×10^{-11}**	1.14×10^{-12}	**200**
TN3 03520	484.3	484.3	3.3	8.3	2.5	2495	8/10	**4.70×10^{-11}**	1.16×10^{-12}	**228**
TN3 03994	479.6	479.6	3.3	8.3	2.5	2353	9/10	**5.90×10^{-11}**	1.46×10^{-12}	**226**
TN3 04513	474.4	474.4	2.3	5.8	1.7	2500	10/10	**8.30×10^{-11}**	1.43×10^{-12}	**253**
TN3 04778	471.8	471.8	2.8	7.0	2.1	2166	8/10	**8.00×10^{-11}**	1.68×10^{-12}	**287**
TN3 05260	466.9	466.9	3.2	8.0	2.4	1958	9/10	**5.70×10^{-11}**	1.37×10^{-12}	**236**
TN3 05514	464.4	464.4	3.2	8.0	2.4	2228	7/10	**4.10×10^{-11}**	9.84×10^{-13}	**266**
TN3 06010	459.4	459.4	3.2	8.0	2.4	2746	9/10	**5.90×10^{-11}**	1.42×10^{-12}	**285**
TN3 06256	457.0	457.0	3.3	8.3	2.5	2346	10/10	**5.90×10^{-11}**	1.46×10^{-12}	**289**
TN3 06765	451.9	451.9	3.4	8.5	2.6	2221	9/10	**4.30×10^{-11}**	1.10×10^{-12}	**305**
TN3 07250	447.0	447.0	3.5	8.8	2.6	2368	9/10	**4.50×10^{-11}**	1.18×10^{-12}	**325**

Table 6. (continued)

Sample	Elevation, m	Corrected Elevation, m	θ, %	ω_θ, %	ω_{geoch}, %	R/W, g L^{-1}	Data mod/exp	D_p, m^2 s^{-1}	D_e, m^2 s^{-1}	$[Cl^-]_{I.W.}$, mg L^{-1}
TN3 07496	444.6	444.6	3.5	8.8	2.6	2490	10/10	**4.60×10^{-11}**	1.21×10^{-12}	**323**
TN3 07980	439.7	439.7	3.5	8.8	2.6	2690	9/10	**5.10×10^{-11}**	1.34×10^{-12}	**298**
TN3 08265	436.9	436.9	3.4	8.5	2.6	2140	9/10	**4.60×10^{-11}**	1.17×10^{-12}	**326**
TN3 08780	431.7	431.7	3.3	8.1	2.4	2537	8/10	**3.70×10^{-11}**	9.02×10^{-13}	**367**
TN3 09250	427.0	427.0	3.3	8.3	2.5	2255	9/10	**4.10×10^{-11}**	1.01×10^{-12}	**305**
TN3 09535	424.2	424.2	3.3	8.3	2.5	1938	9/10	**4.50×10^{-11}**	1.11×10^{-12}	**427**
TN3 10012	419.4	419.4	3.3	8.3	2.5	2014	9/10	**3.90×10^{-11}**	9.65×10^{-13}	**475**
TN3 10500	414.5	414.5	3.3	8.3	2.5	2229	10/10	**4.40×10^{-11}**	1.09×10^{-12}	**491**
TN3 10765	411.9	411.9	3.2	8.0	2.4	2294	10/10	**4.80×10^{-11}**	1.15×10^{-12}	**447**
TN3 11040	409.1	409.1	3.7	9.3	2.8	2070	10/10	**5.90×10^{-11}**	1.64×10^{-12}	**435**
TN3 11485	404.7	404.7	3.9	9.6	2.9	1919	10/10	**6.70×10^{-11}**	1.93×10^{-12}	**582**
TN3 12018	399.4	399.4	3.2	8.0	2.4	2419	9/10	**8.30×10^{-11}**	1.99×10^{-12}	**464**
TN3 12465	394.9	394.9	4.0	10.0	3.0	2088	9/10	**6.70×10^{-11}**	2.01×10^{-12}	**539**
TN3 12735	392.2	392.2	3.5	8.8	2.6	2240	9/10	**7.30×10^{-11}**	1.92×10^{-12}	**798**
TN3 13255	387.0	387.0	3.5	8.8	2.6	2279	10/10	**6.60×10^{-11}**	1.73×10^{-12}	**427**
TN3 13870	380.8	380.8	3.0	7.5	2.3	2236	9/10	**9.30×10^{-11}**	2.09×10^{-12}	**403**
TN3 14295	376.6	376.6	2.2	5.5	1.7	2152	9/10	**6.20×10^{-11}**	1.02×10^{-12}	**640**
TN3 14752	372.0	372.0	2.2	5.5	1.7	2366	9/10	**3.30×10^{-11}**	5.45×10^{-13}	**695**
TN3 15061	368.9	368.9	2.2	5.5	1.7	2011	10/10	**2.90×10^{-11}**	4.79×10^{-13}	**561**
VF2 00439	512.3	505.3	3.00	7.5	2.2	1767	5/5	5.20×10^{-11}	1.17×10^{-12}	**369**
VF2 00848	508.2	501.2	2.98	7.4	2.2	1785	5/5	5.50×10^{-11}	1.23×10^{-12}	**322**
VF2 01298	503.7	496.7	2.67	6.7	2.0	2077	2/5	4.90×10^{-11}	9.81×10^{-13}	**443**
VF2 01574	500.9	494.0	2.55	6.4	1.9	1903	5/5	4.90×10^{-11}	9.35×10^{-13}	**611**
VF2 01915	497.5	490.6	2.66	6.6	2.0	2022	4/5	4.60×10^{-11}	9.18×10^{-13}	**550**
VF3 00444	512.2	505.3	2.99	7.5	2.2	1860	5/5	5.20×10^{-11}	1.17×10^{-12}	**347**
VF3 00885	507.8	500.9	2.57	6.4	1.9	2355	3/5	5.50×10^{-11}	1.06×10^{-12}	**386**
VF3 01250	504.2	497.2	2.73	6.8	2.0	1920	5/5	4.90×10^{-11}	1.00×10^{-12}	**462**
VF3 01630	500.4	493.4	2.85	7.1	2.1	1901	2/5	4.90×10^{-11}	1.05×10^{-12}	**555**
VF3 01929	497.4	490.4	2.97	7.4	2.2	1915	4/5	4.60×10^{-11}	1.02×10^{-12}	**371**
VF4 00406	512.6	505.6	3.37	8.4	2.5	1890	4/5	5.20×10^{-11}	1.31×10^{-12}	**189**
VF4 00845	508.2	501.3	3.39	8.5	2.5	2107	4/5	5.50×10^{-11}	1.40×10^{-12}	**162**
VF4 01240	504.3	497.3	3.41	8.5	2.6	2092	3/5	5.50×10^{-11}	1.41×10^{-12}	**221**
VF4 01618	500.5	493.5	3.23	8.1	2.4	2401	2/4	4.90×10^{-11}	1.19×10^{-12}	**340**
VF4 02000	496.7	489.7	3.37	8.4	2.5	2041	3/5	4.60×10^{-11}	1.16×10^{-12}	**330**
VF4 02440	492.3	485.3	3.49	8.7	2.6	2193	3/5	4.70×10^{-11}	1.23×10^{-12}	**293**
VF4 02735	489.3	482.4	3.32	8.3	2.5	2358	4/5	4.70×10^{-11}	1.17×10^{-12}	**340**
VF4 03240	484.3	477.3	2.99	7.5	2.2	2383	3/5	5.90×10^{-11}	1.32×10^{-12}	**384**
VF4 03640	480.3	473.3	3.13	7.8	2.3	1931	4/5	8.30×10^{-11}	1.95×10^{-12}	**307**
VF4 04010	476.6	469.6	3.24	8.1	2.4	2913	4/5	5.70×10^{-11}	1.39×10^{-12}	**352**
VF4 04444	472.2	465.3	3.09	7.7	2.3	2163	4/5	4.10×10^{-11}	9.50×10^{-13}	**329**
VF4 04840	468.3	461.3	3.24	8.1	2.4	2201	4/5	5.90×10^{-11}	1.43×10^{-12}	**341**
VF4 05170	465.0	458.0	3.19	8.0	2.4	2316	3/5	5.90×10^{-11}	1.41×10^{-12}	**371**
VF4 05600	460.7	453.7	3.31	8.3	2.5	2131	2/5	4.30×10^{-11}	1.07×10^{-12}	**506**
VF4 06050	456.2	449.2	3.15	7.9	2.4	2610	2/5	4.40×10^{-11}	1.04×10^{-12}	**408**
VF4 06070	456.0	449.0	3.15	7.9	2.4	2272	8/13	1.60×10^{-11}	3.78×10^{-13}	**495**
VF4 06445	452.2	445.3	2.98	7.5	2.2	2661	3/5	4.50×10^{-11}	1.01×10^{-12}	**308**
VF4 06465	452.0	445.1	3.13	7.8	2.3	2266	7/12	2.10×10^{-11}	4.93×10^{-13}	**519**
VF4 06840	448.3	441.3	2.63	6.6	2.0	2392	4/5	4.60×10^{-11}	9.08×10^{-13}	**454**
VF4 06875	447.9	441.0	3.11	7.8	2.3	2267	7/12	2.10×10^{-11}	4.89×10^{-13}	**530**
VF4 07240	444.3	437.3	2.78	6.9	2.1	2671	4/5	4.60×10^{-11}	9.58×10^{-13}	**405**
VF4 07260	444.1	437.1	3.11	7.8	2.3	2265	10/13	9.00×10^{-12}	2.10×10^{-13}	**531**
VF4 07616	440.5	433.5	2.73	6.8	2.0	2639	5/5	3.70×10^{-11}	7.57×10^{-13}	**367**
VF4 07670	440.0	433.0	2.50	6.3	1.9	2270	10/13	7.00×10^{-12}	1.31×10^{-13}	**496**
VF4 07914	437.5	430.6	2.92	7.3	2.2	2886	4/5	3.70×10^{-11}	8.11×10^{-13}	**409**

[a]Chloride concentrations and diffusion coefficients obtained by the PECH protocol are bold; other values of D_p are linearly interpolated (according to depth of the sample).

data. Nonetheless, the order of magnitude obtained for diffusion coefficients can be considered correct, in view the homogeneity of the whole data set.

5. Chloride Profile in the Tournemire Argillites

5.1. Data Acquisition

[62] The PECH protocol was applied to borehole TN1 and TN3 samples collected approximately every 4 m; chloride diffusion coefficients and chloride concentrations were determined. The resultant values constitute a 162-m sequence of data, only interrupted at the level of the tunnel (Table 6).

[63] Chloride concentrations of intermediate samples from borehole TN1 have been measured, using a D_p obtained by linear interpolation between previously obtained D_p values for surrounding samples in the sequence.

[64] Additionally, chloride concentrations for boreholes VF2, VF3 and VF4 samples were assessed using only 5

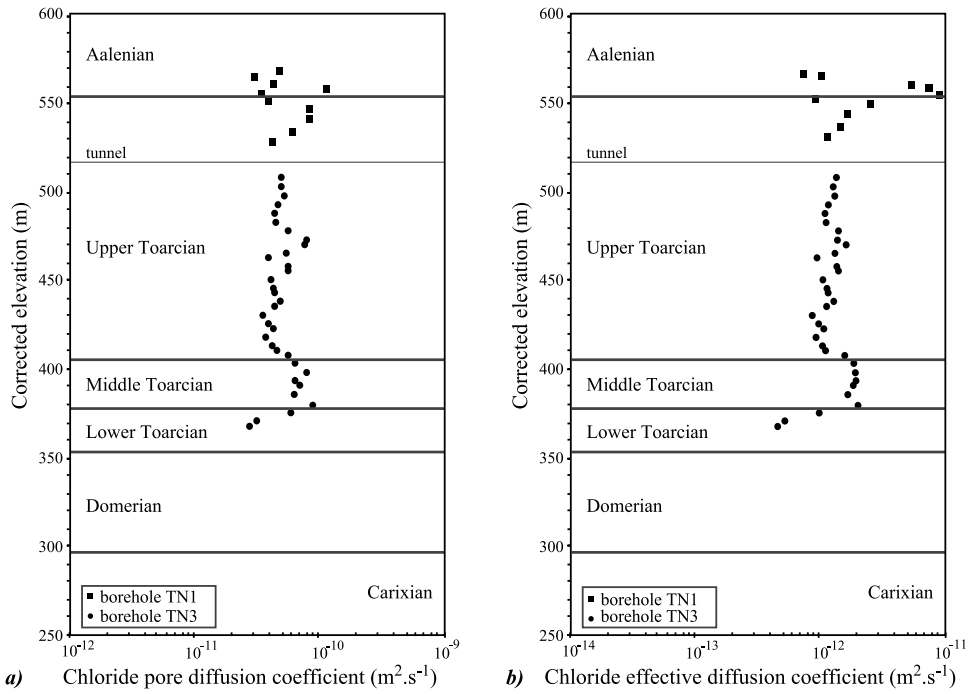

Figure 12. Profiles of (a) the pore diffusion coefficient and (b) the effective diffusion coefficient for chloride in the Tournemire massif.

water samples during the diffusion experiments. Although diffusion coefficients are in a good agreement with those determined for borehole TN3 samples, only 1 or 2 water samples were collected during the transient part of the diffusion. As a result, values for D_p for boreholes VF2, VF3 and VF4 samples should not be used in further work. However, concentrations were determined with generally better precision (more samples were collected over the steady state part of the diffusion experiments) and are included in the study of mass transport (see part 2).

5.2. Reliability of Method: Comparison With Results on Other Clay Materials

[65] Chloride pore diffusion coefficients in argillites and marls are all in the same order of magnitude (Figure 12a) varying between 2×10^{-11} and 9×10^{-11} m^2 s^{-1} (effective diffusion coefficients vary from 3×10^{-13} to 3×10^{-12} m^2 s^{-1}; Figure 12b). This means that the chloride pore diffusion coefficient is about two orders of magnitude less than the value of the chloride diffusion coefficient D_0 in pure water (1.71×10^{-9} m^2 s^{-1} in the work of *Li and Gregory* [1974]). This difference reflects the pore tortuosity in the material and possibly the effect of the variation in the chemical composition of water.

[66] Few measurements of diffusion coefficients have been performed on natural clayey materials having porosities less than 10%, and studies dealing with natural clay materials use a wide range of diffusion coefficients. For instance, while *Hendry et al.* [2000] use a D_e of 1.6×10^{-10} m^2 s^{-1} in the Snakebite Member (a plastic clay with an effective porosity equal to 14%) of the Bearpaw Formation, which is in agreement with *Barone et al.* [1990] and *Barone et al.* [1992], *Hendry and Schwartz* [1988] use a D_e of 6×10^{-12} m^2 s^{-1} for the Colorado shale (with an effective porosity equal to 7%). Often, the threshold values of 6.3×10^{-11} and 5×10^{-10} m^2 s^{-1} given by *Desaulniers et al.* [1981] are cited as the valid values for chloride D_e, omitting the fact that these values are directly based on porosities ranging between 25% and 50%. However, chloride diffusion coefficients presented herein still remain lower than those described in the literature, perhaps reflecting how atypical the Tournemire material really is.

[67] This affirmation is reinforced by measurements of effective iodide diffusion coefficients. In high-density materials, chloride and iodide have very similar behavior with respect to diffusion [*Kozaki et al.*, 1998; *Sato et al.*, 1992]. Iodide D_e measurements performed using diffusion-permeation experiments [*Pocachard et al.*, 1998] range between 1.4 and 2.4×10^{-13} m^2 s^{-1}, and reflect the extremely slow diffusion properties for chemical species in Tournemire argillites and marls. *Rübel and Sonntag* [2001] also describe a low helium diffusion D_p value of 3.5×10^{-11} m^2 s^{-1} in the Opalinus Clay (in which total porosity is 12 to 19%). Considering that helium diffuses at a higher rate than chloride in pure water, it is not surprising that chloride has similar or smaller diffusion coefficients than helium in a media with a smaller and probably more tortuous porosity.

5.3. Discussion on Chloride Transport in the Tournemire Argillites

[68] The vertical profile of pore water chloride concentrations obtained by PECH, for the VF2, VF3, VF4, TN1 and TN3 borehole samples increases downward across the Toarcian units (Figure 13).

[69] The lack of data in the Carixian precludes description of chloride concentrations of interstitial water in the lower part of the sequence. However, low chloride content of the water circulating in the Carixian karstic aquifer suggests a decrease with depth of chloride concentration in the Domerian. Chloride concentrations of Carixian waters are lower

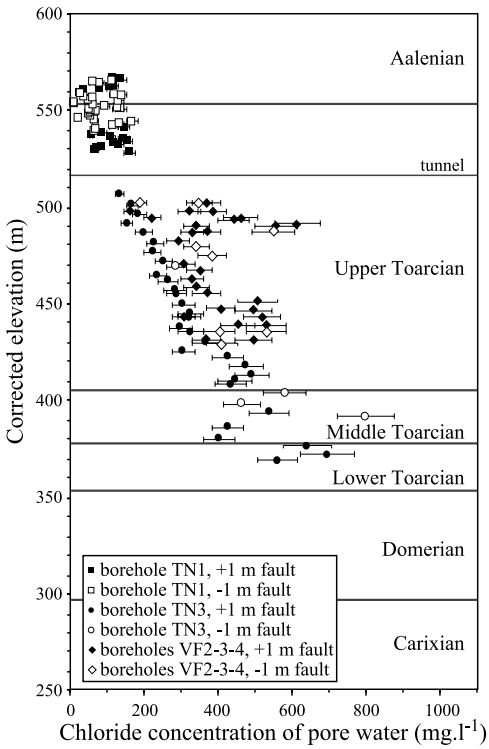

Figure 13. Profile of pore water chloride concentration (error bars represent ±10 %) in the Tournemire massif obtained using the PECH protocol.

than 10 mg L^{-1} [*Barbreau and Boisson*, 1994; *De Windt et al.*, 1999]. The chloride concentration of water circulating in the Aalenian karst is also very low, ranging from 7.3 to 7.7 mg L^{-1} [*Patriarche*, 2001].

[70] Thus, at the Tournemire site, interstitial water of argillites is more concentrated in chloride that water circulating at the argillite boundaries, in the Aalenian and Carixian aquifers. This concentration contrast might result in chloride diffusion from the argillites at a scale of the entire geological sequence. Such processes would explain the shape of the chloride concentration profile, where chloride content increases with depth in the Toarcian layer prior to an expected decrease with depth in the vicinity of the Carixian layer.

[71] On the basis of these data, it seems apparent that mass transport by diffusion could be the main process that controls chloride concentration across the Tournemire massif. It would also imply that water in aquifers bounding the argillites has a very low chloride concentration and that condition has persisted over a significant amount of geologic time and that interstitial water in argillites was initially concentrated in chloride because sediment deposition occurred in marine settings.

[72] This model will be tested (part 2 of this study) using numerical simulations in order to check its validity according to the geological history of the massif and to experimental chloride diffusion coefficients.

6. Conclusion

[73] The development of a specific protocol for obtaining representative chloride data in interstitial water of Tournemire argillites was presented. Diffusion experiments were performed checking that chloride obtained by these diffusion experiments was originally coming from interstitial water and that the process for accessing to this chloride is really diffusion. In order to do so, chemical analyses (ICP-AES, AAS...), X-ray diffractometry analyses and SIMS analyses were performed on argillite samples. A large number of chemical analyses (ionic chromatography) of the water, where chemical equilibration occurred over time during diffusion experiments were also performed. A principal component analysis on this large data set helped to recognize that chloride extracted during the equilibration was obtained by diffusion.

[74] The use of a numerical code for modeling the diffusion during these diffusion experiments yielded to the assessment of initial chloride pore water concentrations (based on steady state of diffusion), and chloride pore diffusion coefficients (based on transient state of diffusion).

[75] The number and the quality of data acquired using the protocol PECH allowed for drawing of the vertical profiles of chloride diffusion coefficients (Figures 12a and 12b) and chloride concentration (Figure 13) of pore water throughout the Tournemire sequence.

[76] The very low chloride effective diffusion coefficients and the shape of the chloride concentration profile suggest then, that diffusion is the main process for mass transport. In order to check whether this hypothesis is in agreement with the geological history of the Tournemire massif, numerical modeling based on these data is presented in part 2 of this article.

Notation

θ	water content in weight, %.
ω_t	true total porosity, %.
ω_θ	total porosity derived from water content, %.
ω_e	effective porosity where advection and dispersion occurs, %.
ω_d	diffusion porosity for a chemical species, %.
ω_{geoch}	geochemical porosity for a chemical species, %.
D_p	pore diffusion coefficient, $m^2\ s^{-1}$.
D_e	effective diffusion coefficient, $m^2\ s^{-1}$.
z	elevation, m.
z_c	corrected elevation (boreholes TN1 and TN3 taken as reference), m.
K	hydraulic conductivity, $m\ s^{-1}$.
P_e	Peclet number.
U	Darcy velocity, $m\ s^{-1}$.
k	permeability, m^2.
μ	dynamic viscosity of the fluid, $kg\ m^{-1}\ s^{-1}$.
D_0	diffusion coefficient of a chemical species in free-water, $m^2\ s^{-1}$.
h	hydraulic head, m.
C	concentration, $mol\ L^{-1}$.
W	volume of added water in diffusion experiments, L.
R	rock mass, g.
V	volume of water sample removed during diffusion experiments, L.

[77] **Acknowledgments.** We wish to thank Sabine Huet-Taillanter and André Raulo for the analytical and technical support, and Louis Raimbault for performing SIMS analyses, as well as Laurent De Windt for his support during the project. The authors also wish to thank two anonymous reviewers, the Associate Editor and Bruce H. Wilkinson for their very helpful comments on this paper. We are grateful to the IRSN for

financing this project, and we greatly appreciated the support provided by Maria Clara Castro during the completion of this article.

References

Barbreau, A., and J.-Y. Boisson (1994), Caractérisation d'une formation argileuse: Résultats obtenus à partir du tunnel de Tournemire de janvier 1992 à juin 1993, *FI/2WCT91/0115*, Comm. à l'Energie Atomique, Inst. de Prot. et de Sûreté Nucl., Fontenay-aux-Roses, France.

Barescut, J. C., and J.-L. Michelot (1997), Constraints on transport in the Tournemire clay site, *J. Contam. Hydrol.*, *26*, 71–79.

Barone, F. S., R. K. Rowe, and R. M. Quigley (1990), Laboratory determination of chloride diffusion coefficient in an intact shale, *Can. Geotech. J.*, *27*, 177–184.

Barone, F. S., R. K. Rowe, and R. M. Quigley (1992), Estimation of chloride diffusion coefficient and tortuosity factor for mudstone, *J. Geotech. Eng.*, *118*(7), 1031–1046.

Beaudoing, G., S. Moutin, M. Launay, and B. Dubing (1996), Coefficients de diffusion et de perméation (dP = 1,5 MPa) d'eau à travers des échantillons d'argile du site de Tournemire, *96/32*, Comm. à l'Energie Atomique, Dép. des Appl. et de la Métrol. des Rayonnements Ionisants, Grenoble, France.

Boisson, J.-Y., J. Cabrera, L. Bertrand, and J.-F. Heitz (1998a), Mesures de très faibles perméabilités in situ et en laboratoire, sur les argilites de Tournemire (Aveyron)—Méthodologies comparées et effet d'échelle, *Bull. Soc. Geol. Fr.*, *169*(4), 1–4.

Boisson, J.-Y., J. Cabrera, and L. De Windt (1998b), Etude des écoulements dans un massif argileux, laboratoire souterrain de Tournemire, *Rep. EUR 18338*, Eur. Comm., Luxembourg.

Boisson, J.-Y., J. Cabrera, and L. De Windt (1998c), Investigating faults and fractures in argillaceous Toarcian formation at the IPSN Tournemire research site, in *Fluid Flow Through Faults and Fractures in Argillaceous Formations: Proceedings of a Joint NEA/EC Workshop*, pp. 207–222, Organ. for Econ. Co-operation and Dev., Paris.

Boisson, J.-Y., L. Bertrand, J.-F. Heitz, and Y. Moreau-Le Golvan (2001), In situ and laboratory investigations of fluid flow trough an argillaceous formation at different scales of space and time, Tournemire tunnel, southern France, *Hydrogeol. J.*, *9*, 108–123.

Bonin, B. (1998), Deep geological disposal in argillaceous formations: Studies at the Tournemire test site, *J. Contam. Hydrol.*, *35*, 315–330.

Bredehoeft, J. D., and S. S. Papadopulos (1980), A method for determining the hydraulic properties of tight formations, *Water Resour. Res.*, *16*(1), 233–238.

Brookins, D. G. (1984), *Geochemical Aspects of Radioactive Waste Disposal*, 347 pp., Springer-Verlag, New York.

Cabrera, J. (1992), Etude structurale des milieux granitiques, schisteux et argileux et les relations avec la perméabilité—Etude structurale dans le milieu argileux: LEMI du Tunnel de Tournemire, rapport et annexes, *Rap. Cont. 6162*, Comm. à l'Energie Atomique, Inst. de Prot. et de Sûrete Nucl., Fontenay-aux-Roses, France.

Cabrera, J., C. Beaucaire, G. Bruno, L. De Windt, A. Genty, N. Ramanbasoa, A. Rejeb, and S. Savoye (2001), Le projet Tournemire comme support de l'expertise sur le stockage profond en milieu argileux: Synthèse des programmes de recherche, *Rep. 01/19*, Inst. de Prot. et de Sûrete Nucl., Fontenay-aux-Roses, France.

Cave, M. R., S. Reeder, D. C. Entwistle, P. A. Blackwell, J. K. Trick, J. Wragg, and S. R. Burden (1997), Chemical characterisation of squeezed pore-waters and aqueous leachates in shales from the Tournemire tunnel, France, *Rep. WI/97/6C*, Br. Geol. Surv., Keyworth, U. K.

Cordier, E., and P. Goblet (1999), Programme METIS—Simulation d'écoulement et de transport miscible en milieu poreux et fracturé—Notice d'emploi, *Rep. LHM/RD/99/18*, Cent. d'Inf. Géol., Ecole Natl. Supérieure des Mines de Paris, Fontainebleau, France.

Dazy, F., J.-F. Le Barzic, G. Saporta, F. Lavallard, and Groupe d'étude et de réflexion interrégional (1996), *L'Analyse des Données Évolutives: Méthodes et Applications*, 227 pp., Technip, Paris.

de Marsily, G. (1986), *Quantitative Hydrogeology*, 440 pp., Academic, San Diego, Calif.

Desaulniers, D. E., J. A. Cherry, and P. Fritz (1981), Origin, age and movement of pore water in argillaceous Quaternary deposits at four sites in southwestern Ontario, *J. Hydrol.*, *50*, 231–257.

De Windt, L., J. Cabrera, and J.-Y. Boisson (1999), Etude géochimique des propriétés de confinement de la formation argileuse de Tournemire, *Rep. DPRE/SERGD/99/17*, Inst. de Prot. et de Sûreté Nucl., Fontenay-aux-Roses, France.

Eggenkamp, H. G. M. (1998), The stable isotope geochemistry of halogens Cl and Br: A review of 15 years development, *Mineral. Mag. A*, *62*, 411–412.

Falck, W. E., A. H. Bath, and P. J. Hooker (1990), Long term solute migration profiles in clay sequences, *Z. Dtsch. Geol. Ges.*, *141*, 415–426.

Fletcher, P., and G. Sposito (1989), The chemical modelling of clay/electrolyte interactions for montmorillonite, *Clay Miner.*, *24*, 375–391.

Fritz, S. J., and I. W. Marine (1983), Experimental support for a predictive osmotic model of clay membranes, *Geochim. Cosmochim. Acta*, *47*, 1515–1522.

Goblet, P. (1989), Programme METIS—Simulation d'écoulement et de transport miscible en milieu poreux et fracturé—Notice de conception, *Rep. LHM/RD/89/23*, Cent. d'Inf. Géol., Ecole Natl. Supérieure des Mines de Paris, Fontainebleau, France.

Harrington, G. A., A. J. Love, and A. L. Herczeg (2001), Relative importance of physical and geochemical processes affecting solute distributions in a clay aquitard, in *Proceedings of the 10th International Symposium on Water-Rock Interaction*, edited by R. Cidu, pp. 177–180, Swets and Zeitlinger, Lisse, Netherlands.

Hendry, M. J., and F. W. Schwartz (1988), An alternative view on the origin of chemical and isotopic patterns in groundwater from the Milk River Aquifer, Canada, *Water Resour. Res.*, *24*(10), 1747–1763.

Hendry, M. J., L. I. Wassenaar, and T. Kotzer (2000), Chloride and chlorine isotopes (^{36}Cl and δ^{37}Cl) as tracers of solute migration in a thick, clay-rich aquitard system, *Water Resour. Res.*, *36*(1), 285–296.

Hoteit, N., O. Ozanam, and K. Su (2000), Geological radioactive waste disposal project in France; conceptual model of a deep geological formation and underground research laboratory in Meuse/Haute-Marne site, in *Pacific Rocks 2000*: "*Rock Around the Rim*," edited by J. Girard et al., 1257–1264, A. A. Balkema, Brookfield, Vt.

Jolliffe, I. T. (1986), *Principal Component Analysis*, 271 pp., Springer-Verlag, New York.

Keijzer, T. J. S., P. J. Kleingeld, and J. P. G. Loch (1999), Chemical osmosis in compacted clayey material and the prediction of water transport, *Geoenviron. Eng.*, *53*(2), 151–159.

Kharaka, Y. K., and F. A. F. Berry (1973), Simultaneous flow of water and solutes through geological membranes—I. Experimental investigation, *Geochim. Cosmochim. Acta*, *37*, 2577–2603.

Kozaki, T., N. Saito, A. Fujishima, S. Sato, and H. Ohashi (1998), Activation energy for diffusion of chloride ions in compacted sodium montmorillonite, *J. Contam. Hydrol.*, *35*, 67–75.

Lavergne, L., L. Lemée, J. Joffre, and A. Amblès (1997), Géochimie organique de sédiments de Tournemire, *Rap. Cont. 6B 058 910 CEA/IPSN*, Lab. de Chim. 12 Synthèse et Réactivité des Substances Nat., Univ. de Poitiers, Poitiers, France.

Lebon, P., and B. Mouroux (1999), Knowledge of the three French underground laboratory sites, *Eng. Geol.*, *52*, 251–256.

Li, Y.-H., and S. Gregory (1974), Diffusion of ions in sea water and in deep sea sediments, *Geochim. Cosmochim. Acta*, *38*, 703–714.

Maes, N., H. Moors, A. Dierckx, P. De Canniere, and M. Put (1999), The assessment of electromigration as a new technique to study diffusion of radionuclides in clayey soils, *J. Contam. Hydrol.*, *36*(3–4), 231–247.

Malusis, M. A., and C. D. Shackelford (2002), Coupling effects during steady-state solute diffusion through a semipermeable clay membrane, *Environ. Sci. Technol.*, *36*(6), 1312–1319.

Malusis, M. A., C. D. Shackelford, and H. W. Olsen (2001), A laboratory apparatus to measure chemico-osmotic efficiency coefficients for clay soils, *Geotech. Test. J.*, *24*(3), 229–242.

Mennessier, G., and P. Collomb (1983), Carte géologique de la France 1/50000—Millau Larzac Ouest-Roquefort, Bur. Rech. Géol. et Minières, Orléans, France.

Michard, G. (1982), Rôle des anions mobiles dans le transport des éléments par les solutions hydrothermales, *C. R. Acad. Sci. Paris, Ser. II*, *295*, 451–454.

Moreau-Le Golvan, Y. (1997), Traçage isotopique naturel des transferts hydriques dans un milieu argileux de très faible porosité: Les argilites de Tournemire (France), Ph.D. thesis, Univ. Paris-Sud, Orsay, France.

Moreau-Le Golvan, Y., J.-L. Michelot, and J.-Y. Boisson (1997), Stable isotope contents of porewater in a claystone formation (Tournemire, France): Assessment of the extraction technique and preliminary results, *Appl. Geochem.*, *12*, 739–745.

Neuzil, C. E. (1994), How permeable are clays and shales?, *Water Resour. Res.*, *30*(2), 145–150.

Nolin, L. (1997), Influence des anions sur la rétention des radioéléments par des matériaux argileux, Ph.D. thesis, Univ. Pierre et Marie Curie (Paris VI), Paris.

Patriarche, D. (2001), Caractérisation et modélisation des transferts de traceurs naturels dans les argilites de Tournemire, Ph.D. thesis, Ecole Natl. Supérieure des Mines de Paris, Fontainebleau, France.

Patriarche, D., E. Ledoux, J.-L. Michelot, R. Simon-Coinçon, and S. Savoye (2004), Diffusion as the main process for mass transport in very low water content argillites: 2. Fluid flow and mass transport modeling, *Water Resour. Res.*, *40* doi:10.1029/2003WR002700, in press.

Pearson, F. J. (1999), What is the porosity of a mudrock?, in *Muds and Mudstones: Physical and Fluid Flow Properties*, edited by A. C. Aplin, A. J. Fleet, and J. H. S. Macquaker, *Geol. Soc. Spec. Publ.*, 158, 9–21.

Pocachard, J., D. Mourzagh, and B. Dubing (1998), Etude de la diffusion de l'iode et de l'eau tritiée à travers des échantillons du site de Tournemire, *Rep. 98.07/JP/CR*, Comm. à l'Energie Atomique, Dép. des Appl. et de la Métrol. des Rayonnements Ionisants, Grenoble, France.

Put, M. J., M. Monsecour, A. Fonteyne, and H. Yoshida (1991), Estimation of the migration parameters for the Boom clay formation by percolation experiments on undisturbed clay cores, in *Materials Research Society Symposium Proceedings: Scientific Basis for Nuclear Waste Managment XIV*, edited by T. A. J. Abrajano and L. H. Johnson, pp. 823–829, Mater. Res. Soc., Warrendale, Pa.

Raimbault, L. (2000), Images ioniques des argilites de Tournemire $^{35}Cl^-$, $^{31}P^-$, $^{19}F^-$, $^{1}H^-$, $^{16}O^-$, $^{28}Si^-$, $^{32}S^-$, $^{12}C^-$, *Rep. LHM/RD/00/35*, Cent. d'Inf. Géol., Ecole Natl. Supérieure des Mines de Paris, Fontainebleau, France.

Reeder, S., M. R. Cave, D. C. Entwistle, and J. K. Trick (1998), Extraction of water and solutes from clayey material: A review and critical discussion of available techniques, *Rep. WI/98/4C*, Br. Geol. Surv., Keyworth, U. K.

Rübel, A., and C. Sonntag (2001), Profiles of noble gases and stable isotopes across the Opalinus Clay at Mont Terri, Switzerland, in *Proceedings of the 10th International Symposium on Water-Rock Interaction*, edited by R. Cidu, pp. 1367–1370, Swets and Zeitlinger, Lisse, Netherlands.

Sacchi, E., J.-L. Michelot, and H. Pitsch (2000), *Porewater Extraction From Argillaceous Rocks for Geochemical Characterisation—Methods and Interpretation*, Nucl. Energy Agency, Organ. for Econ. Co-operation and Dev., Paris.

Sacchi, E., J.-L. Michelot, H. Pitsch, P. Lalieux, and J.-F. Aranyossy (2001), Extraction of water and solutes from argillaceous rocks for geochemical characterisation: Methods, processes, and current understanding, *J. Hydrogeol.*, *9*, 17–33.

Sato, H., T. Kohara, M. Yui, and N. Sasaki (1992), Effect of dry density on diffusion of some radionuclides in compacted sodium bentonite, *J. Nucl. Sci. Technol.*, *29*(9), 873–882.

Sonnenthal, E. L., and G. S. Bodvarsson (1999), Constraints on the hydrology of the unsaturated zone at Yucca Mountain, NV from three-dimensional models of chloride and strontium geochemistry, *J. Contam. Hydrol.*, *38*, 107–156.

Stone, W. J. (1992), Paleohydrological implications of some deep soilwater chloride profiles, Murray Basin, South Australia, *J. Hydrol.*, *132*, 201–223.

Stuckless, J. S., and W. W. Dudley (2002), The geohydrologic setting of Yucca Mountain, Nevada, *Appl. Geochem.*, *17*(6), 659–682.

Toulhoat, P. T., J. P. Gallien, D. Louvat, V. Moulin, P. l'Henoret, P. Guerin, E. Ledoux, I. Gurban, J. A. T. Smellie, and A. Winberg (1996), Preliminary studies of groundwater flow and migration of uranium isotopes around the Oklo natural reactors (Gabon), *J. Contam. Hydrol.*, *21*, 3–17.

Tyler, S. W., J. B. Chapman, S. H. Conrad, D. P. Hammermeister, D. O. Blout, J. J. Miller, M. J. Sully, and J. M. Ginanni (1996), Soil-water flux in the southern Great Basin, United States: Temporal and spatial variations over the last 120,000 years, *Water Resour. Res.*, *32*(6), 1481–1499.

van der Kamp, G., D. R. Van Stempvoort, and L. I. Wassenaar (1996), The radial diffusion method: 1. Using intact cores to determine isotopic composition, chemistry, and effective porosities for groundwater in aquitards, *Water Resour. Res.*, *32*(6), 1815–1822.

Wang, J., C. F. Tsang, T. N. Narisimhan, and P. A. Witherspoon (1977), Transient flow in tight fractures, paper presented at First Invitational Well-Testing Symposium, Berkeley Natl. Lab., Berkeley, Calif.

E. Ledoux, Ecole Nationale Supérieure des Mines de Paris, UMR 7619 Sisyphe 35, rue Saint Honoré, 77305 Fontainebleau Cedex, France.

J.-L. Michelot, OrsayTerre, FRE 2566 CNRS, Faculté des Sciences, Université de Paris-Sud, Bât. 504, 91405 Orsay Cedex, France.

D. Patriarche, Department of Geological Sciences, University of Michigan, 2534 C. C. Little Building, Ann Arbor, MI 48109-1063, USA. (delfpat@umich.edu)

S. Savoye, Institut de Radioprotection et de Sûreté Nucléaire, BP 17, 92262 Fontenay-aux-Roses Cedex, France.

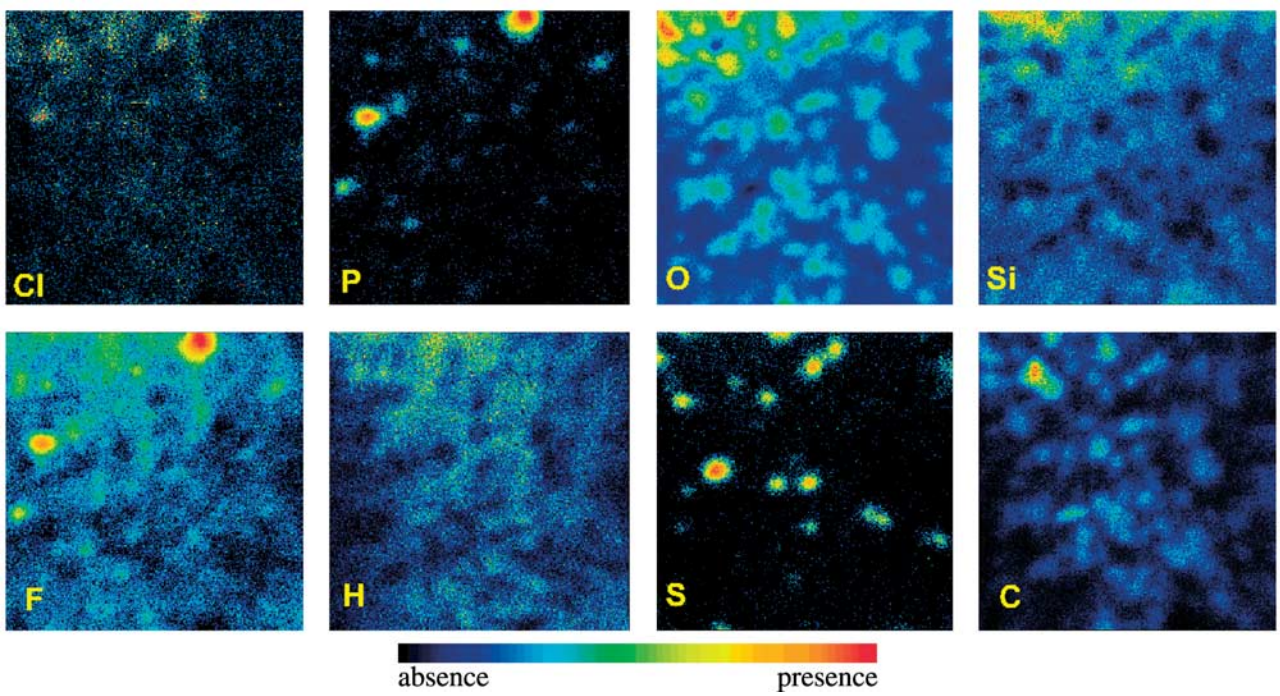

Figure 6. Distribution of chloride, phosphorus, fluoride, hydrogen, oxygen, silica, sulfur, and carbon obtained by SIMS analysis of sample VF4 07670 (sector D); 250 × 250 μm scan [*Raimbault*, 2000].